



Tahyz Gomes Pinto

**Pressure-pressure convolution as a technique
to analyze pressure behavior for injectivity tests
based on a radially composite model**

Tese de Doutorado

Thesis presented to the Programa de Pós-graduação em Matemática, do Departamento de Matemática da PUC-Rio in partial fulfillment of the requirements for the degree of Doutor em Matemática.

Advisor : Prof. Sinesio Pesco
Co-advisor: Prof. Abelardo Borges Barreto Junior

Rio de Janeiro
September 2023



Tahyz Gomes Pinto

**Pressure-pressure convolution as a technique
to analyze pressure behavior for injectivity tests
based on a radially composite model**

Thesis presented to the Programa de Pós-graduação em Matemática da PUC-Rio in partial fulfillment of the requirements for the degree of Doutor em Matemática. Approved by the Examination Committee:

Prof. Sinesio Pesco

Advisor

Departamento de Matemática – PUC-Rio

Prof. Abelardo Borges Barreto Junior

Co-advisor

Departamento de Matemática – PUC-Rio

Prof. Adolfo Puime Pires

Universidade Estadual Norte Fluminense – UENF

Dra. Angélica Nardo Caseri

BASF – Matriz São Paulo

Dr. Eduardo da Silva Castro

Laboratório Nacional de Computação Científica – LNCC

Profa. Malú Grave

Departamento de Engenharia Civil – UFF

Rio de Janeiro, September 14, 2023

All rights reserved.

Tahyz Gomes Pinto

Graduated in mathematics from the Fluminense Federal University in 2015 and a master of mathematics from Pontifical Catholic University in 2019.

Bibliographic data

Pinto, Tahyz Gomes

Pressure-pressure convolution as a technique to analyze pressure behavior for injectivity tests based on a radially composite model / Tahyz Gomes Pinto; advisor: Sinesio Pesco; co-advisor: Abelardo Borges Barreto Junior. – 2023.

69 f: il. color. ; 30 cm

Tese (doutorado) - Pontifícia Universidade Católica do Rio de Janeiro, Departamento de Matemática, 2023.

Inclui bibliografia

1. Matemática – Teses. 2. Testes de injetividade. 3. Análise de transiente de pressão. 4. Reservatórios radialmente compostos. 5. Convolução pressão-pressão. 6. Funções de Green. I. Pesco, Sinesio. II. Barreto Jr., Abelardo Borges. III. Pontifícia Universidade Católica do Rio de Janeiro. Departamento de Matemática. IV. Título.

CDD: 004

Acknowledgments

I have been fortunate to receive guidance, encouragement, support, and immeasurable love, care, and affection throughout my academic journey. I want to express my deepest gratitude to all who were part of this and helped me bring this study to fruition.

I am profoundly grateful to my advisors, Sinesio Pesco and Abelardo Barreto, for their invaluable mentorship and supervision. Their expertise enriched the quality of this work. They are devoted to their students, and it was a pleasure to work with each one of them.

Thanks to all my friends in the Mathematics Department at PUC-Rio, especially those from LPMAC. Each of you is amazing, and you have left part of yourselves with me. During times when I thought about giving up, I took you as an example and stayed strong.

I sincerely thank the fantastic admin team, including Kátia, Creuza, Mariana, and Carlos, from technical support. Your patience, commitment, and care have saved us from countless difficulties.

I would like to acknowledge the PUC-Rio Mathematics Department for providing me with the necessary resources and an enriching academic environment that fostered my intellectual growth and learning.

I cherish the memory of my beloved parents, José Otávio and Rita de Cássia. You are the role models whose love and guidance have shaped my academic journey. Even though you are no longer here in person, our shared memories strengthen me and always inspire me to persevere.

Thank you to my parents-in-law, Neinha and José Antônio, my sister-in-law Ana Júlia, and my brother Raphael. You provided me with a caring and welcoming environment in challenging moments. I am sincerely grateful for it.

Finally, I want to thank the person who has been by my side all this time. Thank you for your support. Thank you for believing in me. Thank you for being there for me even through the toughest of circumstances. My beloved companion, Thiago Silva, I couldn't have done this without you. Thank you for all your help, patience, and the times you believed in me more than myself.

I thank Petrobras for the financial assistance.

This study was financed in part by the Coordenação de Aperfeiçoamento de Pessoal de Nível Superior - Brasil (CAPES) - Finance Code 001

Abstract

Pinto, Tahyz Gomes; Pesco, Sinesio (Advisor); Barreto Jr., Abelardo Borges (Co-Advisor). **Pressure-pressure convolution as a technique to analyze pressure behavior for injectivity tests based on a radially composite model.** Rio de Janeiro, 2023. 69p. Tese de Doutorado – Departamento de Matemática, Pontifícia Universidade Católica do Rio de Janeiro.

The injectivity test is a conventional technique in reservoir engineering used for oil recovery and formation evaluation. Typically, water is injected to displace the existing oil by increasing the pressure in the pores. In this test, the pressure response measurement provides valuable information about the reservoir parameters, including permeability data. Therefore, researchers aim to develop mathematical equations that could accurately model pressure response during these tests for reservoir management and maintenance prediction purposes. This work introduces a new analytical solution for injectivity test analysis. The solution combines the pressure-pressure convolution technique with a two-zone radial model. It allows the evaluation of the injectivity test without precise flow rate data, as the pressure-pressure convolution exclusively uses the pressure data acquired at different positions in the reservoir. The reservoir model comprises an injector well in the inner zone of the reservoir and an observation well in the outer zone for measuring pressure response. The proposed solution was validated by comparing the analytical results with those obtained from a finite differences-based commercial simulator.

Keywords

Injectivity test; Pressure transient analysis; Radially composite reservoir; Pressure-pressure convolution; Green's function.

Resumo

Pinto, Tahyz Gomes; Pesco, Sinesio; Barreto Jr., Abelardo Borges. **Análise do comportamento da pressão em testes de injetividade utilizando convolução pressão-pressão em um reservatório radialmente composto**. Rio de Janeiro, 2023. 69p. Tese de Doutorado – Departamento de Matemática, Pontifícia Universidade Católica do Rio de Janeiro.

Teste de injetividade é uma técnica convencional em engenharia de reservatórios, utilizada para a recuperação de óleo em reservatórios e avaliação de formações. Geralmente utiliza-se água como fluido injetado, que resulta em um deslocamento do óleo presente devido ao aumento da pressão nos poros. Durante o teste, a resposta de pressão medida fornece diversas informações sobre os parâmetros do reservatório, tal como dados de permeabilidade. Desta forma, pesquisadores têm se dedicado em encontrar equações matemáticas que modelam a resposta de pressão desses testes com objetivo de gerenciamento e manutenção preditiva do reservatório. Neste trabalho, apresentamos uma nova solução analítica para a análise de testes de injetividade, que combina a técnica de convolução pressão-pressão com um modelo radial composto de duas zonas. Essa solução permite avaliar o teste de injetividade mesmo na ausência de dados precisos de vazão, uma vez que a convolução pressão-pressão utiliza exclusivamente os dados de pressão adquiridos em diferentes posições do reservatório. O modelo considerado consiste em dois poços, um injetor, localizado na zona interna do reservatório, e um observador, na zona externa. A validação da solução proposta foi realizada por meio da comparação dos resultados analíticos com aqueles obtidos em um simulador comercial baseado em diferenças finitas.

Palavras-chave

Testes de injetividade; Análise de transiente de pressão; Reservatórios radialmente compostos; Convolução pressão-pressão; Funções de Green.

Table of contents

1	Introduction	14
2	Mathematical Framework for Pressure-Pressure Convolution Analysis	19
2.1	Convolution Description	19
2.2	Pressure-Rate Convolution Description	20
2.3	Pressure-Pressure Convolution Description	22
3	Pressure-Pressure Convolution for a Single-Phase Flow in a Composite Reservoir	25
4	Pressure-Pressure Convolution for a Two-Phase Flow	34
5	Results and Discussion	40
5.1	Comparing the Results of the Line-Source Scenario	40
5.1.1	Example 1	41
5.1.2	Example 2	45
5.2	Comparing the Results of the Heterogeneous Scenario	48
5.2.1	Example 1	49
5.2.2	Example 2	52
5.3	Comparing the Results of the Two-Phase Scenario	55
6	Conclusion and future work	60
	Bibliography	62
A	Derivation of the Pressure-Pressure Convolution Equations	66
B	The Auxiliary Problem for Green's Function	68

List of figures

- Figure 2.1 General illustration of a convolution operation of two functions, x and g . The independent variable t represents time and is replaced by the function τ to distinguish it from the time variable in the output function. The kernel function g is mirrored and translated along the time axis by substituting τ with $t - \tau$. Then, the kernel is moved across the input function x for each value of t , and at each time position, $x(\tau)$ and $g(t - \tau)$ are multiplied. The integral of this product over the entire domain represents the output function $y(t)$. The shaded area refers to the interaction region between the two functions. 20
- Figure 2.2 Duhamel's integral scheme: a unit impulse force $\delta(t)$, is applied to a linear system G . It results in an impulse response $g(t)$. This impulse response makes it possible to determine an outcome $y(t)$ for any arbitrary input force $x(t)$. 21
- Figure 2.3 Two-dimensional representation of a circular reservoir with two wells separated by a distance D . 23
- Figure 3.1 Two-region radially composite reservoir scheme. 25
- Figure 3.2 Source location 28
- Figure 3.3 Two-well interference test scheme in a heterogeneous system: active and observation wells configuration. 32
- Figure 4.1 Two-phase radial flow scheme. 34
- Figure 4.2 Two-well interference test scheme during a two-phase flow. 35
- Figure 5.1 Semi-log plot comparing dimensionless pressure values in an infinite homogeneous reservoir for the Example 5.1.1. The graph presents the results from [19] and this work, calculated by Equations (3-32) and (3-34), in a two-well system. 42
- Figure 5.2 Log-log plot of dimensionless pressure derivative vs. time for active and observation well in an infinite homogeneous reservoir for the Example 5.1.1. 43
- Figure 5.3 Log-log plot of the \mathcal{G} -function and the logarithmic derivative $t\mathcal{G}$ -function vs. time for two-well testing in an infinite homogeneous reservoir for the Example 5.1.1. 45
- Figure 5.4 Semi-log plot comparing dimensionless pressure values in an infinite homogeneous reservoir for the Example 5.1.2. The graph presents the results from [19] and this work. 46
- Figure 5.5 Log-log plot of dimensionless pressure derivative vs. time for active and observation well in an infinite homogeneous reservoir for the Example 5.1.2. 47
- Figure 5.6 Log-log plot of the \mathcal{G} -function and the logarithmic derivative $t\mathcal{G}$ -function vs. time for two-well testing in an infinite homogeneous reservoir for the Example 5.1.2. 48

Figure 5.7	Semi-logarithmic plot comparing the dimensionless pressure values for a two-well interference testing in an infinite heterogeneous reservoir for the Example 5.2.1. The plot shows the results from the reservoir simulator solution alongside the outcomes generated by the proposed model for an infinite heterogeneous reservoir.	50
Figure 5.8	Log-log plot of dimensionless pressure derivative vs. time for active and observation well in interference testing in an infinite heterogeneous reservoir for the Example 5.2.1.	51
Figure 5.9	Log-log plot of the \mathcal{G} -function and the logarithmic derivative $t\mathcal{G}$ -function vs. time for a two-well interference testing in an infinite heterogeneous reservoir for the Example 5.2.1.	52
Figure 5.10	Semi-logarithmic plot comparing the dimensionless pressure values for a two-well interference testing in an infinite heterogeneous reservoir for the Example 5.2.2. The plot includes results from the reservoir simulator and the outcomes for an infinite heterogeneous reservoir obtained from the proposed model.	53
Figure 5.11	Log-log plot of dimensionless pressure derivative vs. time for active and observation well in a two-well interference testing in an infinite heterogeneous reservoir for the Example 5.2.2.	54
Figure 5.12	Log-log plot of the \mathcal{G} -function and the logarithmic derivative $t\mathcal{G}$ -function vs. time for a two-well interference testing in an infinite heterogeneous reservoir for the Example 5.2.2.	55
Figure 5.13	Semi-logarithmic plot comparing the dimensionless pressure values for a two-well interference testing in an infinite homogeneous reservoir during two-phase flow for the Example 5.3. The plot includes results from the reservoir simulator and those from an infinite two-phase system obtained from the proposed model.	56
Figure 5.14	Log-log plot of dimensionless pressure derivative vs. time for a two-well interference testing in an infinite homogeneous reservoir during two-phase flow for the Example 5.3.	58
Figure 5.15	Log-log plot of the \mathcal{G} -function and the logarithmic derivative $t\mathcal{G}$ -function vs. time for a two-well interference testing in an infinite homogeneous reservoir during two-phase flow for the Example 5.3.	59

List of tables

Table 5.1	Reservoir properties for a scenario involving single-phase flow in a homogeneous medium.	41
Table 5.2	Reservoir properties for heterogeneous medium.	49
Table 5.3	Reservoir properties for a homogeneous medium under two-phase flow.	56

List of Symbols

GF – *Green's Function*

IC – *Initial Condition*

IBC – *Internal Boundary Condition*

OBC – *Outer Boundary Condition*

ODE – *Ordinary Differential Equation*

P-R – *Pressure-Rate*

P-P – *Pressure-Pressure*

PCC – *Pressure Continuity Condition*

PDE – *Partial Differential Equation*

RCC – *Rate Continuity Condition*

Nomenclature

α_p - Unit conversion factor

A_m, B_m, C_m, D_m - Coefficients in the pressure solution system equation

c_{t_j} - Total system compressibility of region j

c_{r_j} - Rock compressibility of region j

δ - Dirac delta function

Δp_j - Pressure change of region j

Δp_{jD} - Dimensionless pressure change of region j

$\Delta \bar{p}_{jD}$ - Laplace transform of dimensionless pressure change of region j

η_j - Hydraulic diffusivity of region j

$G_{i,j}$ - Greens function of the i th region due to the source in the j th region

$\bar{G}_{i,j}$ - Laplace transform of Greens function of the i th region due to the source in the j th region

\mathcal{G} - P-p convolution *kernel*

$\bar{\mathcal{G}}$ - Laplace transform of p-p convolution *kernel*

h - Reservoir thickness

I_i, K_i - Modified Bessel functions of first and second kind and order i

κ_j - Permeability of region j

κ_{r_j} - Relative permeability of fluid j

\mathcal{L} - Laplace operator

p_i - Initial Pressure

p_j - Pressure response of region j

p_{jD} - Dimensionless pressure response of region j

ϕ_i - Porosity of region j

q - Flow rate

q_{sf} - Sandface flow rate

q_1 - Flow rate at active well

\bar{q}_1 - Laplace transform of flow rate at active well

r - Radius

r' - Source radius

r_1 - Interface radius

r_e - Reservoir outer radius

r_f - Waterfront radius

r_w - Wellbore radius

r_D - Dimensionless radius
 r'_D - Dimensionless source radius
 r_{1D} - Dimensionless interface radius
 r_{eD} - Dimensionless reservoir outer radius
 r_{fD} - Dimensionless waterfront radius
 S_o - Oil saturation
 S_{or} - Residual oil saturation
 S_w - Water saturation
 S_{wi} - Irreducible water saturation
 t - Time
 t' - Source time position
 t_D - Dimensionless time
 t'_D - Dimensionless source time position
 u - Laplace variable
 W_j - Well in region j
 μ - Fluid viscosity
 μ_j - Viscosity of region j
 λ_j - Fluid mobility of region j

1

Introduction

An injectivity test is a strategy to acquire reservoir information by analyzing the pressure transient data gathered during fluid injection. The injected fluid is crucial in pressurizing the reservoir and extending its longevity [1]. It is common to use water as the injected fluid in this process. When water is injected into the pores, it increases pressure and displaces the existing oil. The water then stays in the pores along with the remaining oil, maintaining the reservoir's pressure. As the water progresses, it gradually produces a water-flooded area surrounding the injector well. Consequently, two distinct regions with different fluid properties are formed: the water and oil banks.

Over the years, reservoir engineering researchers have dedicated their efforts to developing models that can efficiently simulate this system's configuration. Analytical models under different conditions were constructed to characterize the reservoir pressure response and offer insight into geological attributes.

For instance, Abbaszadeh and Kamal (1989) [2] introduced a methodology that assesses injectivity and fall-off within a single-layer oil reservoir subject to water flooding. The study formulates analytical solutions, incorporating relative permeability, wellbore storage, and skin factors to elucidate pressure and saturation distributions. Barreto Jr., Peres, and Pires (2011) [3] discussed an analytical solution for a vertical water injection well in a layered oil reservoir with an infinite extent. The solution can compute wellbore pressure, injection rates, and waterfront for each layer without numerical flow simulators. The methodology also offers potential for parameter estimation using field data when a production logging rate profile is accessible. Peres et al. (2004) [5] developed approximate analytical pressure solutions for a vertical well with restricted entry and a non-equidistant horizontal well. The solutions incorporated a multiphase term and utilized models with Buckley-Leverett equations to account for a two-phase zone and the movement of the waterfront. In injectivity testing for completed horizontal wells, Peres and Reynolds (2003) [4] developed an approximate analytical solution to ascertain wellbore pressure in oil-bearing reservoirs. One can observe that data collection during the injectivity test contributes to an enhanced comprehension of the reservoir's

attributes and enables the estimation of parameters such as permeability and porosity.

In the well-testing literature, the radially composite scheme is a widely used method for describing heterogeneity within a reservoir [6, 7, 8, 9]. The model comprises a set of concentric circles. Each circle has a unique radius, creating enclosed zones between every two circles, known as annuli. The reservoir heterogeneity is produced by defining each created area with different rock or fluid properties.

Loucks and Guerrero (1961) [10] proposed a theoretical model to explain pressure drop behavior in a two-zone composite reservoir with distinct permeabilities in each zone. The model established the pressure drop variation in the internal region with time intervals, permeabilities, and inner circle radius. Additionally, they developed a strategy for pressure distribution applicable to short and extended periods for all zones. Similarly, Satman (1985) [11] suggested an analytical study focused on interference tests in a composite reservoir. The study analyzes the pressure response observed at the monitoring well in the reservoir's outer region. The proposed solution contemplated a constant flow rate, wellbore storage effects, and the skin factor at the active well. Also, it employed the type-curve technique to estimate the relevant reservoir parameters. Olarewaju and Lee (1987) [6] offered solutions for interpreting transient pressure tests conducted in finite and infinite-acting composite reservoirs. Their solutions described the constant rate and pressure behaviors observed during such tests. Moreover, they suggest interpreting pressure and pressure derivative type curves, considering the effects of wellbore storage. Furthermore, their study introduces the application of the composite reservoir model to fractured wells. Thompson and Reynolds (1997) [12] investigated the pressure-transient behavior in reservoirs with radial heterogeneity for single-phase and multiphase flows. They examine their findings using heterogeneous gas-condensate reservoirs and explore other multiphase flow issues. Recently, Yan *et al.* (2021) [13] investigated the impact of sand migration, stress sensitivity, and high-viscosity oil on the pressure behavior of weakly consolidated offshore sand reservoirs. They classify the reservoir into two zones based on the changes in permeability resulting from sand production. The researchers proposed a model that combines the discrete boundary and discrete wellbore approaches with the boundary-element method.

As shown by [2, 12, 14], the radially composite approach is often used in studies on injectivity tests to simulate the fluid bank arrangements. Neto *et al.* (2020) [15] proposed a method for evaluating wellbore pressure during injectivity tests. They use a piston-like flow and a radially composed reservoir

model that accommodates scenarios where the reservoir is subject to two-phase flow, delineated into water and oil regions, or even expands to encompass three distinct regions with a damaged zone near the well, referred to as the skin zone. The study of Bela *et al.* (2022) [16] presented a novel concept involving an impulse function for two-phase flow in single-layer reservoirs with vertical wells. They used a radially composite reservoir approach to show the waterfront propagation and assumed a piston-like fluid displacement. The impulse function was later applied to determine pressure change in multilayer reservoirs with different layer properties and single-layer reservoirs with horizontal wells.

The previous studies primarily relied on flow rate data to investigate heterogeneous and two-phase systems. However, an alternative technique, presented by Goode *et al.* (1991) [17], called pressure-pressure convolution (p-p convolution), exclusively depending on pressure data, has been introduced and implemented in the realm of well-testing literature. Their method involves a new interpretation for the multiprobe tester, identifying flow regimes using pressure readings from observation probes. A reliable flow regime identification process is crucial for multiple probe formation testers due to local heterogeneities and changes near the wellbore, including permeability variations, shale barriers, and saturation effects, significantly affecting the observed pressure response. Usually, the flow rate history needs to be known for model identification. Nevertheless, the flow rate can be challenging to control and maintain constant. Thus, they use p-p convolution to determine the flow regime and data quality when the flow rate history is unknown.

A comprehensive study by Onur *et al.* (2004) [18] examined multiprobe and packer-probe pressure-transient tests considering diverse p-p convolutions combinations for single and multi-layered reservoir systems. They also derived approximate equations that can be used during spherical and radial flow for a vertical well in a single-layered system. These equations indicate which parameter can be uniquely determined by using p-p convolution. On the other hand, they showed that p-p convolution analysis sometimes may not yield unique parameter estimates. As a result, they provided a technique that checks the validity of the parameter estimate obtained from p-p convolution analysis.

In the existing literature on p-p convolution and deconvolution, a notable contribution was made by Kuchuk *et al.* (2010) [19]. They have compiled a comprehensive overview of formation evaluation and well-testing analysis covering a broad range of topics, including flow regimes, convolution, deconvolution, and estimation of reservoir nonlinear parameters. Specifically, their study of p-p convolution investigates its usage in various testing techniques,

including multiwell pressure transient testing and wireline formation testing.

One significant aspect highlighted is the disparity between flow rate measurements conducted at the surface and wellbore pressure measurements taken from the downhole. This discrepancy suggests that the accuracy of flow rate data may be compromised by uncertainties related to surface separator conditions. Furthermore, researchers have demonstrated that wellbore storage substantially impacts interference and pulse test measurements. The p-p convolution is a valuable tool to mitigate these factors and reduce uncertainties. For more information, see [19] and the references therein.

In addition, pressure measurements are typically obtained with high accuracy, so p-p convolution becomes valuable for formulating solutions for flow regime identification. Numerous studies have examined the p-p convolution technique, contributing to a better understanding of this methodology. However, several studies focused on homogeneous systems, limiting their exploration of a reservoir's inherent heterogeneity and failing to account for the diverse range of factors in real-world scenarios.

To the best of the author's knowledge, most existing literature on the pressure-pressure convolution technique focuses on homogeneous systems operating under single-phase flow. In contrast, this study aims to extend this method by applying it to heterogeneous systems under a single-phase flow and homogeneous systems under a two-phase flow. This study employs the pressure-pressure convolution technique and two-zone composite model to analyze pressure behavior in an infinite radially composite reservoir system during two-well interference tests. The well-testing context comprises two wells: one active and one observation well. The observation well is used to monitor pressure changes during production or injection. Analyzing the pressure response in the observation well makes it possible to identify the flow regime and estimate the reservoir parameters. A novel analytical solution is presented by deriving a Green function to account for reservoir heterogeneity in pressure-pressure convolution. The impulse response calculation is essential for applying the convolution method since it allows obtaining the system response. Therefore, Green's function is critical to acquiring the impulse response data and then the model interpretation. This method enables analyzing interference tests between two wells without requiring flow rate information. It differs from the study of Kuchuk *et al.* (2010) [19] p-p convolution approach, which assumes homogeneity and applies the line source solution for each well. It also differs from the study of Satman (1985) [11] interference test strategy, which relies on flow data.

Furthermore, the presented formulation is built in the Laplace domain

and inverted numerically to the time domain using the Stehfest algorithm [20]. Numerical experiments were performed to validate the research findings of this study. The proposed model was compared to the methodology proposed by Kuchuk *et al.* (2010) [19] and with a commercial simulator based on finite differences. This comparison successfully demonstrated the applicability of the new approach for analyzing pressure transients in a two-well interference test. The evaluation process involved an analysis of the pressure curves, including the Bourdet derivative assessment [21] to identify the flow regime.

This work is structured as follows: Chapter 2 provides an overview of p-p convolution used in previous studies, including a mathematical background and notations. Chapter 3 describes the proposed theoretical model that utilizes the pressure-pressure convolution technique and the two-zone composite model to analyze pressure behavior for a heterogeneous reservoir. Chapter 4 focuses on advancing this approach, examining its application to a two-phase flow system. Finally, in Chapter 5, the results obtained by applying the suggested approach in Chapters 3 and 4 are discussed.

2

Mathematical Framework for Pressure-Pressure Convolution Analysis

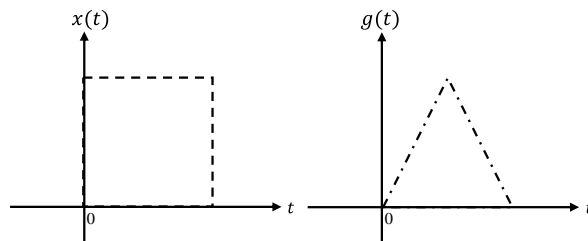
This study presents a new analytical solution using a method based on the convolution operation; therefore, this chapter will provide a brief theory about convolution operation and some of its applications in well-testing literature.

2.1

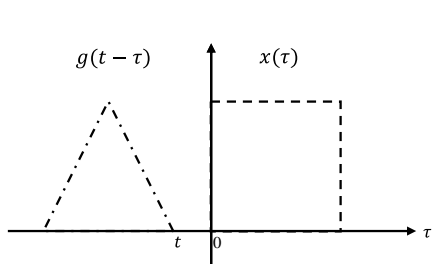
Convolution Description

The mathematical convolution is a linear operation that generates an output function by combining two signals: a kernel and an input function [22]. In this process, the convolution kernel is shifted over the input signal. At each time step t , the kernel and the overlapping part of the input signal are multiplied. This product is then integrated over the entire domain, producing a new signal, the convolution output, that can provide valuable information about the system's behavior [23].

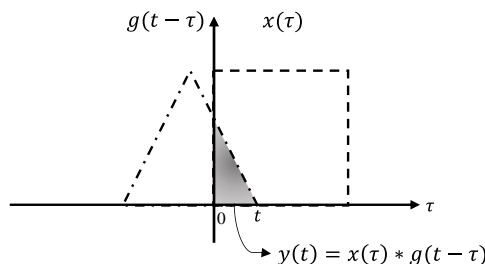
The convolution process is illustrated in Figures 2.1(a)-(c). In Figure 2.1(a), two functions are displayed: the input $x(t)$ and the kernel $g(t)$. Figure 2.1(b) shows $x(\tau)$ and the shifted kernel $g(t - \tau)$. Figure 2.1(c) highlights the area under both x and g resulting from the shifting progression on t that defines the convolution.



2.1(a): Two functions to be convolved.



2.1(b): g is flipped and shifted horizontally by a distance t .



2.1(c): The overlap area between x and g .

Figure 2.1: General illustration of a convolution operation of two functions, x and g . The independent variable t represents time and is replaced by the function τ to distinguish it from the time variable in the output function. The kernel function g is mirrored and translated along the time axis by substituting τ with $t-\tau$. Then, the kernel is moved across the input function x for each value of t , and at each time position, $x(\tau)$ and $g(t-\tau)$ are multiplied. The integral of this product over the entire domain represents the output function $y(t)$. The shaded area refers to the interaction region between the two functions.

The convolution operation can be defined mathematically using the following equation:

$$y(t) = (x * g)(t) = \int_{-\infty}^{+\infty} x(\tau) g(t - \tau) d\tau, \quad (2-1)$$

in which $*$ denotes the convolution operator. Thus, $(x * g)$ symbolizes the convolution of functions x and g at a specific time t . $x(t)$ is an input function, $g(t)$ indicates the kernel, and $y(t)$ represents the output function. The variable τ performs as a shift parameter.

The convolution integral is crucial in analyzing reservoir models, particularly in the well-testing literature. The following sections will demonstrate how this operation can be applied in reservoir engineering.

2.2 Pressure-Rate Convolution Description

In the well-testing literature, the convolution integral is used to analyze the response of a reservoir model due to some force function [24]. One widely

discussed technique is Duhamel’s principle, which offers effective methods for formulating solutions to heat conduction and pressure diffusion problems with time-dependent boundary conditions by using the solution corresponding problem with time-independent boundary conditions [25].

The Duhamel principle constitutes a mathematical method for solving non-homogeneous linear partial differential equations (PDEs). This technique implies decomposing a non-homogeneous forcing function into a series of inputs represented by unit impulses or unit-step functions. It is based on the principle of superposition, wherein the response to a sum of inputs is equal to the sum of individual responses to each input [26, 25]. The problem’s solution is a convolution integral, combining the solution of the corresponding homogeneous PDE with the given forcing function.

Figure 2.2 displays the scheme of Duhamel’s principle approach. In the upper diagrams, it can be noticed that an input function $\delta(t)$, also known as the Dirac delta, is applied to a linear and time-invariant system G . The $\delta(t)$ function mathematically represents an instantaneous unit-impulse in time [27]. The result is the impulse response $g(t)$, the convolution kernel. The lower diagram shows an arbitrary input force, $x(t)$. This input force consists of a combination of impulse functions that are shifted in time. The resulting output $y(t)$ is then obtained by convolving each system impulse response of each time-shifted impulse input. The convolution result is a new function that reflects a system’s linear response.

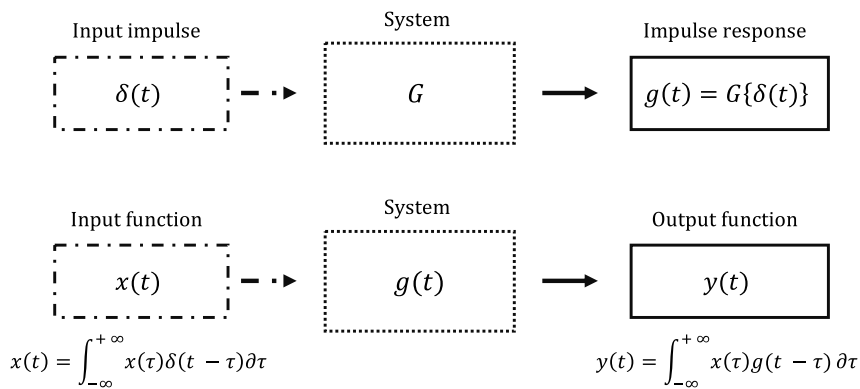


Figure 2.2: Duhamel’s integral scheme: a unit impulse force $\delta(t)$, is applied to a linear system G . It results in an impulse response $g(t)$. This impulse response makes it possible to determine an outcome $y(t)$ for any arbitrary input force $x(t)$.

Duhamel’s principle is commonly used in petroleum engineering literature to determine the wellbore pressure-drop solution for a variable flow rate. This principle involves convolving the unit-rate pressure gradient response of

the reservoir $\left(\frac{\partial p_u}{\partial t}\right)$ with the variable flow rate data (q_{sf}) to produce the wellbore pressure drop (Δp_w) [28, 29, 24]. The method can convert pressure information gathered during variable rates into equivalent data collected during a constant production rate, allowing conventional pressure transient analysis techniques to be used for interpretation [30]. This technique is also called pressure-rate convolution (p-r convolution) [19] and can be mathematically written as:

$$\Delta p_w(r, t) = \int_0^t q_{sf}(\tau) \frac{\partial p_u}{\partial t}(r, t - \tau) d\tau. \quad (2-2)$$

In Equation (2-2), the term p_u refers to the pressure drop at a specific time t , resulting from the constant production of a rate measurement unit. Its time derivative is equivalent to the unit impulse response, $\frac{\partial p_u}{\partial t} \equiv g$.

2.3 Pressure-Pressure Convolution Description

Another convolution-based method in well-testing studies can examine a system's transient pressure behavior employing only pressure functions as convolution operation parameters. This method connects pressure measurements taken at different reservoir or formation locations. This technique, called pressure-pressure convolution analysis (p-p convolution), was initially introduced by Goode et al. [17]. Since then, different studies have focused on this approach in the well-testing literature [18, 31, 19]. The principle of this method lies in the possibility of measuring pressure at two distinct spatial locations apart from the source, as demonstrated by Goode et al. [17]. These pressure regions can be distributed vertically within the formation, such as in a wireline test, or laterally, like in an interference test. So, suppose a Cartesian x-y plane comprising two wells, an active and an observation. In other words, an interference test in an infinite radial model is being considered. Figure 2.3 presents an illustration.

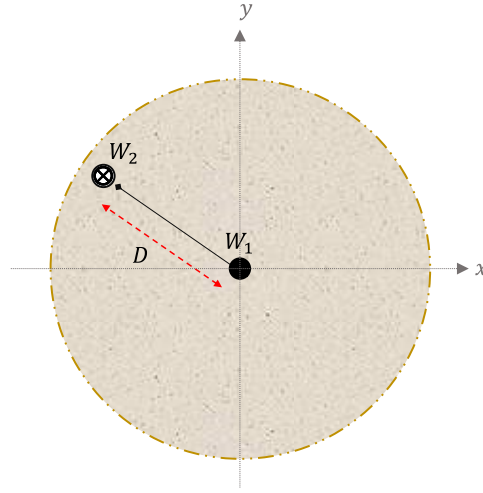


Figure 2.3: Two-dimensional representation of a circular reservoir with two wells separated by a distance D .

The active well (W_1) has a radius $r = r_w > 0$. It is situated at the center of the reservoir, precisely at the origin of the Cartesian axis. In contrast, the observation well (W_2) is located at a distance $r = D$ away from the active well, such that $D > r_w$.

The formulation of p-p convolution derives from the Duhamel principle. Consequently, the method requires knowledge of the kernel or influence function. Thus, as shown in Appendix A, the p-r convolution equation (Equation (2-2)) can be used to find the pressure response at each well for a unit flow rate (see Equations (A-1) and (A-3)). It is computed in the time domain. However, when employing the Laplace transform, the convolution operation simplifies into a scalar product between the input signal and the kernel. This process generates two mathematical expressions in the Laplace domain with common terms, including the flow rate term, as shown in Equations (A-2) and (A-4). The shared terms can be eliminated by dividing one equation by the other, deriving then the following formula to calculate the pressure response at point D through pressure-based functions:

$$\Delta \bar{p}_2(D, u) = \Delta \bar{p}_1(r_w, u) \bar{\mathcal{G}}(r_w, D, u). \quad (2-3)$$

Equation (2-3) represents the overall formula for p-p convolution in the Laplace domain, which connects the pressure responses of active and observation wells. In this equation, u represents the Laplace variable, and the overlined variables indicate that they are in the Laplace domain. Using the inverse operator of the Laplace transform, \mathcal{L}^{-1} , the p-p convolution formulation is identified by:

$$\Delta p_2(D, t) = \int_0^t \Delta p_1(r_w, t - \tau) \mathcal{G}(r_w, D, t) d\tau, \quad (2-4)$$

in which \mathcal{G} , denominated \mathcal{G} -function, is determined as:

$$\mathcal{G} = \mathcal{L}^{-1} \left\{ \frac{\bar{g}_{2,1}(D, u)}{\bar{g}_{1,1}(r_w, u)} \right\}, \quad (2-5)$$

where $\bar{g}(r_w, u)$ and $\bar{g}(D, u)$ are the Laplace transform of unit-impulse response at the active and observation well, respectively. $g(r, t)$ corresponds to a rate-normalized pressure gradient response.

The \mathcal{G} -function refers to the p-p convolution kernel. Based on research from Onur et al. [31] and Goode et al. [17], analyzing the plot of the \mathcal{G} -function can help determine the flow regime and interpretation model needed for parameter estimation through an examination of its log-log curve. However, it is necessary to know the impulse functions of the geometries under study to obtain this information.

Furthermore, the Bourdet derivative [21], also known as log-derivative analysis, is an essential diagnostic tool for data interpretation. For the p-p convolution case, the log-derivative analysis evaluates the log-log signature of $t\mathcal{G}(r, t)$ vs. t .

The proposed model presented in the upcoming chapters utilizes pressure-pressure convolution as an effective method to study pressure diffusion in a radially composite model for two-well interference testing.

Based on these assumptions, the following diffusivity equation describes the flow in each region [6]:

$$\text{PDE: } \frac{1}{r} \frac{\partial}{\partial r} \left(r \frac{\partial p_j(r, t)}{\partial r} \right) - \frac{1}{\eta_j} \frac{\partial p_j(r, t)}{\partial t} = 0, \quad (3-1)$$

in which $j \in \{1, 2\}$. The subscript 1 represents properties in Region I, the inner zone ($r_w \leq r \leq r_1$), and the subscript 2 refers to Region II, the outer zone ($r_1 \leq r$). r_1 is the interface radius separating the two reservoir areas. Hydraulic diffusivity is defined as:

$$\eta_j = \frac{\kappa_j}{\phi_j \mu_j c_{tj}}, \quad (3-2)$$

where μ denotes fluid viscosity. ϕ , κ , and c_t characterize the reservoir porosity, the permeability, and the total compressibility of each region j , respectively.

By employing the subsequent definitions of dimensionless variables in Equations (3-3) to (3-5), the system of partial differential equations can be converted into a dimensionless form.

$$t_D = \frac{\kappa_2 t}{\phi_2 \mu c_{t2} r_w^2}, \quad (3-3)$$

$$r_D = \frac{r}{r_w}, \text{ and} \quad (3-4)$$

$$p_{jD}(r_D, t_D) = \frac{\kappa_2 h}{\alpha_p q \mu} [p_i - p_j(r, t)] \quad \text{with } j \in \{1, 2\} \quad (3-5)$$

The following expressions configure the dimensionless form for the governing equations:

Region I:

$$\frac{1}{r_D} \frac{\partial}{\partial r_D} \left(r_D \frac{\partial p_{1D}(r_D, t_D)}{\partial r_D} \right) - \frac{\eta_2}{\eta_1} \frac{\partial p_{1D}(r_D, t_D)}{\partial t_D} = 0 \quad 1 < r_D < r_{1D} \quad (3-6)$$

Region II:

$$\frac{1}{r_D} \frac{\partial}{\partial r_D} \left(r_D \frac{\partial p_{2D}(r_D, t_D)}{\partial r_D} \right) - \frac{\partial p_{2D}(r_D, t_D)}{\partial t_D} = 0 \quad r_{1D} < r_D \quad (3-7)$$

The applied initial condition is given by:

$$\text{IC: } p_{1D}(r_D, t_D = 0) = p_{2D}(r_D, t_D = 0) = 0 \quad (3-8)$$

The inner and outer boundary conditions are provided, respectively, as:

$$\text{IBC: } \left(r_D \frac{\partial p_{1D}(r_D, t_D)}{\partial r_D} \right) \Big|_{r_D=1} = -\frac{\kappa_2}{\kappa_1} \quad 1 < r_D < r_{1D}, \quad (3-9)$$

$$\text{OBC: } \lim_{r_{eD} \rightarrow \infty} p_{2D}(r_D = r_{eD}, t_D) = 0 \quad r_{1D} < r_D, \quad (3-10)$$

In addition, because of the continuity of pressure and flow rate across the interface between the regions, two interface conditions are associated with the problem [6]. These conditions are specified by:

$$\text{PCC: } p_{1D}(r_{1D}^-, t_D) = p_{2D}(r_{1D}^+, t_D), \quad (3-11)$$

$$\text{RCC: } \left(r_D \frac{\partial p_{1D}(r_D, t_D)}{\partial r_D} \right) \Big|_{r_D=r_{1D}^-} = \frac{\kappa_2}{\kappa_1} \left(r_D \frac{\partial p_{2D}(r_D, t_D)}{\partial r_D} \right) \Big|_{r_D=r_{1D}^+}, \quad (3-12)$$

in this context, PCC stands for Pressure Continuity Condition, and RCC for Rate Continuity Condition.

The solution for a radially composite system using the p-p convolution technique requires knowledge of the response of the physical system to an impulsive force as the kernel of the operation. For this purpose, it is necessary to find GF G that satisfies Equations (3-13) and (3-14).

$$\nabla^2 G(r, r', t, t') = \delta(r - r', t - t') \quad \text{in } \Omega, \quad (3-13)$$

$$G = 0 \quad \text{on } \partial\Omega. \quad (3-14)$$

in which $G(r, r', t, t')$ is the influence experienced at location (r, t) as a result of a source at (r', t') [32]. $\Omega = \{(r, r', t, t') \mid r, r' > 0, t > t' \geq 0\}$.

The GF, denoted as G , is defined as the response of a linear operator to an impulse input. So instead of solving the differential equations in the general form $\hat{L}u(\mathbf{x}) = f(\mathbf{x})$, where \hat{L} is a linear differential operator, and u, f are functions, the solution can be determined since if possible find G that that satisfies Equations (3-13) and (3-14).

Thus, considering a source located in Region I at r' , as depicted in Figure 3.2, the system of equations to derive a formulation for impulse responses can be established by connecting the definition of GF with the dimensionless Equations (3-6) through (3-12), whose results are presented in Appendix B. After employing the Laplace Transform in Equations (B-1) to (B-7), the

mathematical expressions are as ensues:

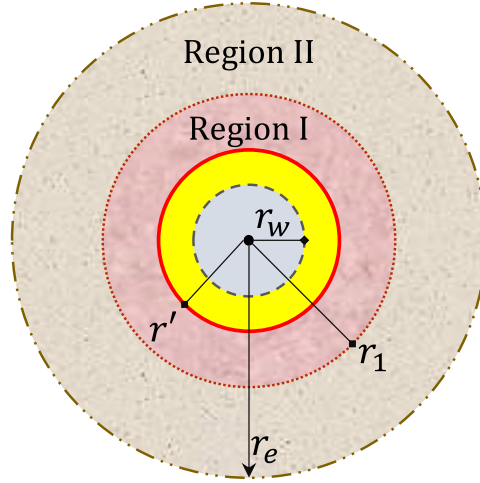


Figure 3.2: Source location

– Region I ($1 < r'_D, r_D < r_{1D}$):

$$\begin{aligned} \frac{1}{r_D} \frac{\partial}{\partial r_D} \left(r_D \frac{\partial \bar{G}_{1,1}(r_D, r'_D, u, t'_D)}{\partial r_D} \right) - \frac{\eta_2}{\eta_1} u \bar{G}_{1,1}(r_D, r'_D, u, t'_D) = \\ = -\frac{\kappa_2}{\kappa_1} \delta(r_D - r'_D) \exp(-ut'_D), \end{aligned} \quad (3-15)$$

$$\text{IBC: } \left(r_D \frac{\partial \bar{G}_{1,1}(r_D, r'_D, u, t'_D)}{\partial r_D} \right) \Big|_{r_D=1} = 0; \quad (3-16)$$

– Region II ($r'_D < r_{1D} < r_D < r_{eD}$):

$$\frac{1}{r_D} \frac{\partial}{\partial r_D} \left(r_D \frac{\partial \bar{G}_{2,1}(r_D, r'_D, u, t'_D)}{\partial r_D} \right) - u \bar{G}_{2,1}(r_D, r'_D, u, t'_D) = 0, \quad (3-17)$$

$$\text{OBC: } \lim_{r_{eD} \rightarrow \infty} \bar{G}_{2,1}(r_D = r_{eD}, r'_D, u, t'_D) = 0; \quad (3-18)$$

– Interface ($r_D = r_{1D}$):

$$\text{PCC: } \bar{G}_{1,1}(r_{1D}^-, r'_D, u, t'_D) = \bar{G}_{2,1}(r_{1D}^+, r'_D, u, t'_D), \quad (3-19)$$

RCC:

$$\left(r_D \frac{\partial \bar{G}_{1,1}(r_D, r'_D, u, t'_D)}{\partial r_D} \right) \Big|_{r_D=r_{1D}^-} = \frac{\kappa_2}{\kappa_1} \left(r_D \frac{\partial \bar{G}_{2,1}(r_D, r'_D, u, t'_D)}{\partial r_D} \right) \Big|_{r_D=r_{1D}^+} \quad (3-20)$$

where u refers to Laplace's variable. $\bar{G}_{1,1}$ denotes the Laplace domain impulse response in Region I because of source positioning in this zone, while $\bar{G}_{2,1}$ is the Laplace domain impulse response in Region II with the source placed in the first region. r'_D represents the dimensionless spatial position of the source.

From the properties of the Dirac delta function, the absence of a source at any point $r_D \neq r'_D$ reduces Equation (3-15) to a homogeneous equation [27]. By definition, Equation (3-17) is also homogeneous. The general representation of these equations is the widely known zero-order modified Bessel equations [33], which possess a general solution given by:

$$\bar{G}_{1,1}(r_D, r'_D, u, t'_D) = \begin{cases} A_1 I_0(r_D z) + B_1 K_0(r_D z) & 1 < r_D < r'_D < r_{1D} \quad (3-21) \\ A_2 I_0(r_D z) + B_2 K_0(r_D z) & r'_D < r_D < r_{1D} \quad (3-22) \end{cases}$$

$$\bar{G}_{2,1}(r_D, r'_D, u, t'_D) = A_3 I_0(r_D \sqrt{u}) + B_3 K_0(r_D \sqrt{u}) \quad r_{1D} < r_D < \infty \quad (3-23)$$

where $I_0(x)$ and $K_0(x)$ correspond to the modified zero-order Bessel function of the first and second kinds. The constants A_m and B_m , in which $m = \{1, 2, 3\}$, must be determined. These coefficients are obtained through boundary and interface conditions and other requirements concerning GF properties. The z factor is defined as:

$$z = \sqrt{\frac{\eta_2}{\eta_1}} u. \quad (3-24)$$

Employing the outer boundary condition, given by Equation (3-18), in Equation (3-23), implies that $A_3 = 0$ [33]. Thus:

$$\bar{G}_{2,1}(r_D, r'_D, u, t'_D) = B_3 K_0(r_D \sqrt{u}) \quad r_{1D} < r_D < \infty. \quad (3-25)$$

Calculating $\partial_{r_D} \bar{G}_{1,1}$ from Equation (3-21) and then applying the inner boundary condition, given by (3-16), yields:

$$A_1 I_1(z) - B_1 K_1(z) = 0. \quad (3-26)$$

Replacing Equations (3-22) and (3-23) and their derivatives (∂_{r_D}) at pres-

sure and rate interface conditions, Equations (3-19) and (3-20), respectively:

$$A_2 I_0(r_{1D} z) + B_2 K_0(r_{1D} z) - B_3 K_0(r_{1D} \sqrt{u}) = 0, \quad (3-27)$$

$$A_2 I_1(r_{1D} z) - B_2 K_1(r_{1D} z) + \frac{\kappa_2}{\kappa_1} \sqrt{\frac{\eta_1}{\eta_2}} B_3 K_1(r_{1D} \sqrt{u}) = 0. \quad (3-28)$$

At $r_D = r'_D$, G function must be continuous [27]. Thus, from Equations (3-21) and (3-22):

$$A_1 I_0(r'_D z) + B_1 K_0(r'_D z) - A_2 I_0(r'_D z) - B_2 K_0(r'_D z) = 0. \quad (3-29)$$

To provide the delta function in Equation (3-13), the first derivative of G must be discontinuous. To obtain this result, one can integrate Equation (3-15) in the interval $(r'_D - \epsilon, r'_D + \epsilon)$, and let $\epsilon \rightarrow 0$. Which leads to:

$$\begin{aligned} \lim_{\epsilon \rightarrow 0} \left[\left(r_D \frac{\partial \bar{G}_{1,1}(r_D, r'_D, t_D, t'_D)}{\partial r_D} \right) \Big|_{r_D=r'_D+\epsilon} \right. \\ \left. - \left(r_D \frac{\partial \bar{G}_{1,1}(r_D, r'_D, t_D, t'_D)}{\partial r_D} \right) \Big|_{r_D=r'_D-\epsilon} \right] \\ = -\frac{\kappa_2}{\kappa_1} \exp(-ut'_D). \quad (3-30) \end{aligned}$$

The function G and its derivative are linear operators. Consequently, the limit in Equation (3-30) can be applied separately to each sum term. The derivatives of Equations (3-21) and (3-22) are used to solve this limit. Therefore, if $r_D = r'_D - \epsilon$, then $r_D < r'_D$, so the left-hand side sum term of Equation (3-30) is replaced by the derivative of Equation (3-21). On the other hand, if $r_D = r'_D + \epsilon$, then $r_D > r'_D$ and the right-hand is substituted by the derivative of Equation (3-22). Hence:

$$\begin{aligned} -A_1 I_1(r'_D z) + B_1 K_1(r'_D z) + A_2 I_1(r'_D z) - B_2 K_1(r'_D z) = \\ -\sqrt{\frac{\eta_1}{\eta_2}} \frac{\kappa_2}{\kappa_1} \frac{\exp(-ut'_D)}{r'_D \sqrt{u}}. \quad (3-31) \end{aligned}$$

Finally, solving the system constructed with Equations (3-26) - (3-29), and (3-31), the constants A_1 , B_1 , A_2 , B_2 , and B_3 may be determined, making it possible to find the answer for G .

Thus, the Laplace transform of the impulse response G in each reservoir region can be written as:

$$\begin{aligned} \bar{G}_{1,1}(r_D, r'_D, u, t'_D) = \\ \frac{\kappa_2}{\kappa_1} \exp(-ut'_D) \left[\frac{I_0(r_D z) K_1(z) + K_0(r_D z) I_1(z)}{K_1(z) f_1 + I_1(z) (-f_2)} \right] [K_0(r'_D z) f_1 + I_0(r'_D z) f_2] \\ 1 < r_D < r'_D < r_{1D}, \quad (3-32) \end{aligned}$$

$$\begin{aligned} \bar{G}_{1,1}(r_D, r'_D, u, t'_D) = \\ \frac{\kappa_2}{\kappa_1} \exp(-ut'_D) \left[\frac{I_0(r'_D z) K_1(z) + K_0(r'_D z) I_1(z)}{K_1(z) f_1 + I_1(z) (-f_2)} \right] [I_0(r_D z) f_2 + K_0(r_D z) f_1] \\ r'_D < r_D < r_{1D}, \quad (3-33) \end{aligned}$$

$$\begin{aligned} \bar{G}_{2,1}(r_D, r'_D, u, t'_D) = \\ \frac{\kappa_2}{\kappa_1} \sqrt{\frac{\eta_1}{\eta_2}} \frac{\exp(-ut'_D)}{r_{1D} \sqrt{u}} \left[\frac{I_0(r'_D z) K_1(z) + K_0(r'_D z) I_1(z)}{K_1(z) f_1 + I_1(z) (-f_2)} \right] K_0(r_D \sqrt{u}) \\ r_{1D} < r_D < \infty, \quad (3-34) \end{aligned}$$

where:

$$f_1 = K_0(r_{1D} \sqrt{u}) I_1(r_{1D} z) + \frac{\kappa_2}{\kappa_1} \sqrt{\frac{\eta_1}{\eta_2}} I_0(r_{1D} z) K_1(r_{1D} \sqrt{u}), \quad (3-35)$$

$$f_2 = K_0(r_{1D} \sqrt{u}) K_1(r_{1D} z) + \frac{\kappa_2}{\kappa_1} \sqrt{\frac{\eta_1}{\eta_2}} K_0(r_{1D} z) K_1(r_{1D} \sqrt{u}). \quad (3-36)$$

The GFs (3-32) - (3-34) give a general formulation for impulse response in a radially composite reservoir with a source in Region I.

Following the two-well system shown in Figure 3.3, one active well at r_{wD} and one observation well at D , the p-p convolution can be defined as proposed by Kuchuk et al. [19]:

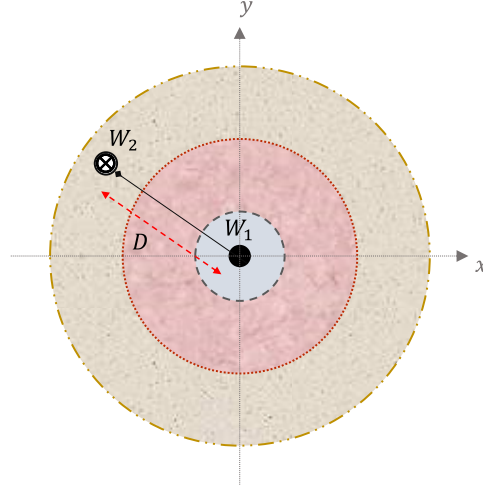


Figure 3.3: Two-well interference test scheme in a heterogeneous system: active and observation wells configuration.

$$\Delta p_{2D}(D, t_D) = \int_0^{t_D} \Delta p_{1D}(1, t_D - \tau) \mathcal{G}(1, D, t_D) d\tau. \quad (3-37)$$

And in the Laplace domain, as follows:

$$\Delta \bar{p}_{2D}(D, u) = \Delta \bar{p}_{1D}(1, u) \bar{\mathcal{G}}(1, D, u). \quad (3-38)$$

The \mathcal{G} -function is obtained from Equation (2-5). Note that, for a composite system, \mathcal{G} is reached from the GF solution at the active and observation well, i.e., by employing $r_D = 1.0$ in Equation (3-32) and $r_D = D$ in Equation (3-34). So, the impulse response solution at W_1 and W_2 is, respectively:

$$\bar{\mathcal{G}}_{1,1}(1, u) = \frac{\kappa_2}{\kappa_1} \exp(-ut'_D) \left[\frac{I_0(z) K_1(z) + K_0(z) I_1(z)}{K_1(z) f_1 + I_1(z) (-f_2)} \right] [K_0(z) f_1 + I_0(z) f_2] \quad (3-39)$$

$$\bar{\mathcal{G}}_{2,1}(D, u) = \frac{\kappa_2}{\kappa_1} \sqrt{\frac{\eta_1}{\eta_2}} \frac{\exp(-ut'_D)}{r_{1D} \sqrt{u}} \left[\frac{I_0(z) K_1(z) + K_0(z) I_1(z)}{K_1(z) f_1 + I_1(z) (-f_2)} \right] K_0(D\sqrt{u}) \quad (3-40)$$

And thus, substituting Equations (3-36) and (3-37) into Equation (2-5) yields:

$$\mathcal{G}(1, D, t_D) = \mathcal{L}^{-1} \left\{ \sqrt{\frac{\eta_1}{\eta_2}} \frac{K_0(D\sqrt{u})}{r_{1D} \sqrt{u} [K_0(z) f_1 + I_0(z) f_2]} \right\} \quad (3-41)$$

Implementing p-p convolution with the provided unit responses allows evaluating the output response and the \mathcal{G} -function.

4

Pressure-Pressure Convolution for a Two-Phase Flow

This chapter discusses the proposed model for applying p-p convolution for a two-phase flow in a homogeneous medium. The system is shaped through a radially composite scheme, similar to the model explored previously in Chapter 3.

During an injectivity test, the oil displacement occurs by water injection. Then, two regions can be formed: the flooded and the unflooded area. The flow in a radial direction creates two concentric banks, one for water and the other for oil. The fluid is uniformly distributed in the space, filling it with a specific volume using the piston flow method. The fluids in each area exhibit different properties, which results in a two-zone radially composite system, as illustrated in Figure 4.1.

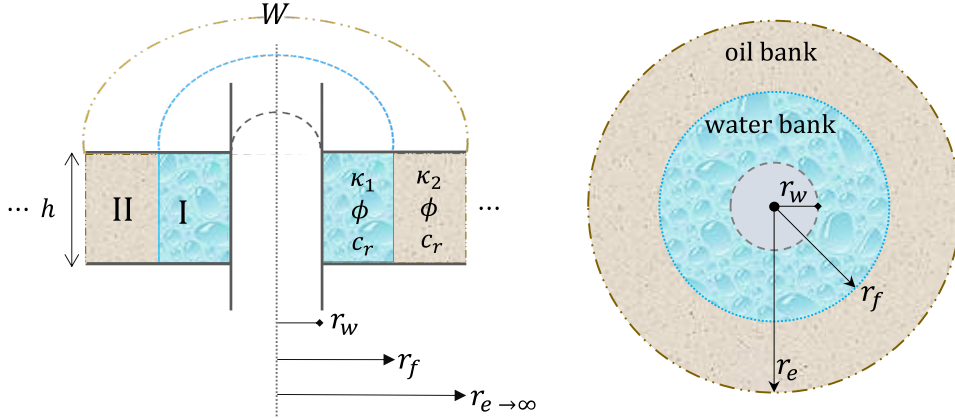


Figure 4.1: Two-phase radial flow scheme.

As water is injected, the flood-front position (denoted as r_f) moves along with its progress. The Buckley-Leverett equation [34] is used to determine the location of the flood-front at each time step and can be seen in Equation 4-1.

$$r_f(t) = \sqrt{r_w^2 + \frac{\int_0^t q_{inj}(\tau) d\tau}{\pi\phi h} f'_w(S_w)}, \quad (4-1)$$

where r_f is called the waterfront radius, the interface radius splitting the two banks in the reservoir. q_{inj} , ϕ , h , and $f'_w(S_w)$ denote the injection flow rate, the

reservoir porosity, the formation thickness, and the fractional flow derivative in this sequence. Based on Equation (4-1), it is noticeable that the interface between the two zones varies over time.

Water movement in the porous medium is assumed to be a piston-like displacement. Initially, the relative permeability of oil is one, i.e., $K_{ro} = 1$, as the medium is completely saturated with oil. In this case, $S_o = 1$, and $S_w = 0$. As the water begins to flow, the flooded bank starts to form. When the medium is filled with water, the water saturation S_w is assumed to be one, i.e., $S_o = 0$ and $S_w = 1$. Consequently, the relative water permeability equals one $K_{rw} = 1$.

As a result, the fractional flow derivative (f'_w) is calculated employing Equation (4-2) [15, 16]:

$$f'_w(S_w) = \frac{1}{1 - S_{wi} - S_{or}}, \quad (4-2)$$

where S_{wi} is the irreducible water saturation and S_{or} the residual oil saturation.

Analogous to the heterogeneous model explained in the previous chapter, the two-phase problem is characterized by a laterally infinite reservoir with two fully penetrated vertical wells. The injection well is located at the water zone in the system's center, while the observation well is in the oil zone. A representation of this model can be found in Figure 4.2.

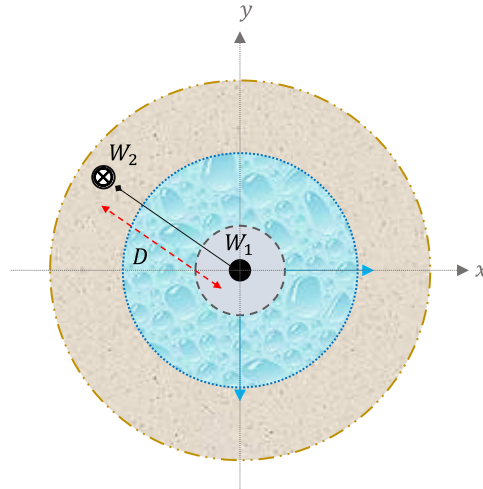


Figure 4.2: Two-well interference test scheme during a two-phase flow.

As discussed in Chapter 3, the present analysis considers an isothermal flow of slightly compressible fluid, adhering to Darcy's law. The reservoir's initial pressure (p_i) and parameters remain uniform and constant. Additionally,

there is no flow resistance between the two regions, and both the skin and the wellbore storage effects have been disregarded.

Equation (3-1) describes the diffusivity equation for each region. In the two-phase model, the subscript j distinguishes between fluid properties. $j = 1$ refers to water bank properties within ($r_w \leq r \leq r_f$), while $j = 2$ represents oil bank properties for ($r_f \leq r$). r_f constitutes the water-oil interface radius.

The hydraulic diffusivity (η_j) is defined as:

$$\eta_j = \frac{\lambda_j}{\phi c_t}, \quad \text{where} \quad \lambda_j = \frac{\kappa \kappa_{rj}}{\mu_j} \quad (4-3)$$

where λ_j refers to fluid mobility. ϕ , c_t , κ , κ_{rj} , and μ_j denote the reservoir's porosity, total compressibility, absolute permeability, fluid relative permeability, and fluid viscosity, respectively.

The dimensionless variables are functions of the oil bank region properties, as demonstrated in Equations (3-3) to (3-5) in the previous chapter. Hence, the system's equations in dimensionless form are determined by:

– Region I ($1 < r_D < r_{fD}$):

$$\frac{1}{r_D} \frac{\partial}{\partial r_D} \left(r_D \frac{\partial p_{1D}(r_D, t_D)}{\partial r_D} \right) - \frac{\eta_2}{\eta_1} \frac{\partial p_{1D}(r_D, t_D)}{\partial t_D} = 0, \quad (4-4)$$

$$\text{IC:} \quad p_{1D}(r_D, t_D = 0) = 0, \quad (4-5)$$

$$\text{IBC:} \quad \left(r_D \frac{\partial p_{1D}(r_D, t_D)}{\partial r_D} \right) \Big|_{r_D=1} = -\frac{\lambda_2}{\lambda_1}; \quad (4-6)$$

– Region II ($r_{1D} < r_D < r_{eD}$):

$$\frac{1}{r_D} \frac{\partial}{\partial r_D} \left(r_D \frac{\partial p_{2D}(r_D, t_D)}{\partial r_D} \right) - \frac{\partial p_{2D}(r_D, t_D)}{\partial t_D} = 0, \quad (4-7)$$

$$\text{IC:} \quad p_{2D}(r_D, t_D = 0) = 0, \quad (4-8)$$

$$\text{OBC:} \quad \lim_{r_{eD} \rightarrow \infty} p_2(r_D = r_{eD}, t_D) = 0; \quad (4-9)$$

– Interface ($r_D = r_{fD}$):

$$\text{PCC: } p_{1D}(r_{fD}^-, t_D) = p_{2D}(r_{fD}^+, t_D), \quad (4-10)$$

$$\text{RCC: } \left(r_D \frac{\partial p_{1D}(r_D, t_D)}{\partial r_D} \right) \Big|_{r_D=r_{fD}^-} = \frac{\lambda_2}{\lambda_1} \left(r_D \frac{\partial p_{2D}(r_D, t_D)}{\partial r_D} \right) \Big|_{r_D=r_{fD}^+}. \quad (4-11)$$

This new formulation analyzes the pressure behavior in a two-phase flow through a homogeneous reservoir using p-p convolution. As stated in this study, obtaining the solution requires knowledge of the impulse response function that characterizes the system's geometry. For this purpose, one must find GFs that satisfy the conditions specified in Equations (3-13) and (3-14). Chapter 3 provides detailed instructions on how to solve the associated Green problem. The same methodology is used for a two-phase model, which comprises the following system of equations:

$$\left\{ \begin{array}{l} C_1 I_1(z) - D_1 K_1(z) = 0, \end{array} \right. \quad (4-12)$$

$$\left\{ \begin{array}{l} C_2 I_0(r_{fD}z) + D_2 K_0(r_{fD}z) - D_3 K_0(r_{fD}\sqrt{u}) = 0 \end{array} \right. \quad (4-13)$$

$$\left\{ \begin{array}{l} C_2 I_1(r_{fD}z) - D_2 K_1(r_{fD}z) + \frac{\lambda_2}{\lambda_1} \sqrt{\frac{\eta_1}{\eta_2}} D_3 K_1(r_{fD}\sqrt{u}) = 0 \end{array} \right. \quad (4-14)$$

$$\left\{ \begin{array}{l} C_1 I_0(r'_D z) + D_1 K_0(r'_D z) - C_2 I_0(r'_D z) - D_2 K_0(r'_D z) = 0 \end{array} \right. \quad (4-15)$$

$$\left\{ \begin{array}{l} -C_1 I_1(r'_D z) + D_1 K_1(r'_D z) + C_2 I_1(r'_D z) - D_2 K_1(r'_D z) = \\ = -\sqrt{\frac{\eta_1}{\eta_2}} \frac{\lambda_2}{\lambda_1} \frac{\exp(-ut'_D)}{r'_D \sqrt{u}} \end{array} \right. \quad (4-16)$$

wherein C_1 , D_1 , C_2 , D_2 , and D_3 are the constants to be determined. u is the Laplace variable. $I_0(x)$ and $K_0(x)$ are the modified zero-order Bessel functions of the first and second kinds, and $I_1(x)$ and $K_1(x)$ are their corresponding derivatives.

The general solution G in Laplace Domain is reached by solving the system shaped by Equations (4-12) through (4-16):

$$\begin{aligned} \bar{G}_{1,1}(r_D, r'_D, u, t'_D) = \\ \frac{\lambda_2}{\lambda_1} \exp(-ut'_D) \left[\frac{I_0(r_D z) K_1(z) + K_0(r_D z) I_1(z)}{K_1(z) f_3 + I_1(z) (-f_4)} \right] [K_0(r'_D z) f_3 + I_0(r'_D z) f_4] \\ 1 < r_D < r'_D < r_{f_D}; \quad (4-17) \end{aligned}$$

$$\begin{aligned} \bar{G}_{1,1}(r_D, r'_D, u, t'_D) = \\ \frac{\lambda_2}{\lambda_1} \exp(-ut'_D) \left[\frac{I_0(r'_D z) K_1(z) + K_0(r'_D z) I_1(z)}{K_1(z) f_3 + I_1(z) (-f_4)} \right] [I_0(r_D z) f_4 + K_0(r_D z) f_3] \\ r'_D < r_D < r_{f_D}; \quad (4-18) \end{aligned}$$

$$\begin{aligned} \bar{G}_{2,1}(r_D, r'_D, u, t'_D) = \\ \frac{\lambda_2}{\lambda_1} \sqrt{\frac{\eta_1}{\eta_2}} \frac{\exp(-ut'_D)}{r_{f_D} \sqrt{u}} \left[\frac{I_0(r'_D z) K_1(z) + K_0(r'_D z) I_1(z)}{K_1(z) f_3 + I_1(z) (-f_4)} \right] K_0(r_D \sqrt{u}) \\ r_{f_D} < r_D < \infty; \quad (4-19) \end{aligned}$$

where:

$$f_3 = K_0(r_{f_D} \sqrt{u}) I_1(r_{f_D} z) + \frac{\lambda_2}{\lambda_1} \sqrt{\frac{\eta_1}{\eta_2}} I_0(r_{f_D} z) K_1(r_{f_D} \sqrt{u}), \quad (4-20)$$

$$f_4 = K_0(r_{f_D} \sqrt{u}) K_1(r_{f_D} z) + \frac{\lambda_2}{\lambda_1} \sqrt{\frac{\eta_1}{\eta_2}} K_0(r_{f_D} z) K_1(r_{f_D} \sqrt{u}). \quad (4-21)$$

Therefore, the pressure unit-response in the Laplace Domain during an injectivity test for an injection and observation wells, respectively, is given by:

$$\bar{G}_{1,1}(1, u) = \frac{\lambda_2}{\lambda_1} \exp(-ut'_D) \left[\frac{I_0(z) K_1(z) + K_0(z) I_1(z)}{K_1(z) f_3 + I_1(z) (-f_4)} \right] [K_0(z) f_3 + I_0(z) f_4] \quad (4-22)$$

$$\bar{G}_{2,1}(D, u) = \frac{\lambda_2}{\lambda_1} \sqrt{\frac{\eta_1}{\eta_2}} \frac{\exp(-ut'_D)}{r_{fD} \sqrt{u}} \left[\frac{I_0(z) K_1(z) + K_0(z) I_1(z)}{K_1(z) f_3 + I_1(z) (-f_4)} \right] K_0(D\sqrt{u}) \quad (4-23)$$

Substituting Equations (4-22) and (4-23) into Equation (2-5) and simplifying the generated expression leads to the \mathcal{G} -function, the p-p convolution kernel for a system characterized by a two-phase flow in a homogeneous reservoir:

$$\mathcal{G}(1, D, t_D) = \mathcal{L}^{-1} \left\{ \sqrt{\frac{\eta_1}{\eta_2}} \frac{K_0(D\sqrt{u})}{r_{fD} \sqrt{u} [K_0(z) f_3 + I_0(z) f_4]} \right\} \quad (4-24)$$

5 Results and Discussion

In order to assess the effectiveness of the model outlined in Chapters 3 and 4, a thorough comparison will be made among the numerical outcomes generated by this new method and the results obtained from existing models in literature and a reservoir simulator's outputs. The objective is to confirm the new approach's reliability and consistency and to validate its accuracy through convergence testing. The inversion of numerical Laplace solutions into the time domain was achieved using the algorithm established by Stehfest (1970) [20].

The model will be evaluated in three stages:

- single-phase flow in a homogeneous medium;
- single-phase flow in a heterogeneous medium;
- two-phase flow in a homogeneous medium.

For the first scenario, it is assumed that the reservoir properties, such as permeability, are uniform throughout the reservoir. The findings presented by Kuchuk et al. [19] will serve as a benchmark for comparison. In the second scenario, each zone within the reservoir has unique properties, while in the third scenario, two zones are formed with differing fluid properties. The results of these scenarios will be compared to a commercial simulator that utilizes finite differences to conduct accurate calculations. For all cases, the wells have a wellbore radius r_w of 0.108 m, the initial pressure p_i is 300.0 kgf/cm², and the model does not consider any storage or skin effects.

5.1 Comparing the Results of the Line-Source Scenario

A scenario is assumed in which the proposed reservoir model is homogeneous, assigning the same attributes to the inner region of the reservoir as those of the outer area. Table 5.1 displays the considered reservoir properties for the homogeneous situation.

Case	Region	κ [mD]	μ [cP]	h [m]	ϕ	c_t [cm^2/kgf]
5.1	I	250	5.1	20	0.25	1.2×10^{-5}
	II					

Table 5.1: Reservoir properties for a scenario involving single-phase flow in a homogeneous medium.

5.1.1

Example 1

The active well was taken from the observation well at a dimensionless distance of $D = 90.0$. The interface radius measures $r_{1D} = 15$. Figures 5.1 and 5.2 illustrate the plot of dimensionless pressure transient behavior and the log-log plot of the dimensionless pressure derivative, respectively, for the formulation suggested in this work as well as the line-source solution derived from [19] for both wells. The outcomes of this proposed model are represented by the dashed line with the circle marker, whereas the solid line denotes the results obtained from [19] formulations.

Results reveal a notable agreement, as seen in Figure 5.1. For the active well solutions ($\Delta P_D^{1,1}$), characterized by black and pink colors, it's possible to see a slight disagreement at initial times. It can be explained due to the unit impulse response function in Equations (3-32) - (3-34) for a source located at $r'_D = 1.0$ and $t'_D = 1.0$. The exponential term is a function of t'_D , and the values are too small in the early stages. So, the pressure behavior changes during initial times because the value is decreased. To the observation well ($\Delta P_D^{2,1}$), the pressure data at a short time is close enough to zero in both formulations, so this difference is negligible.

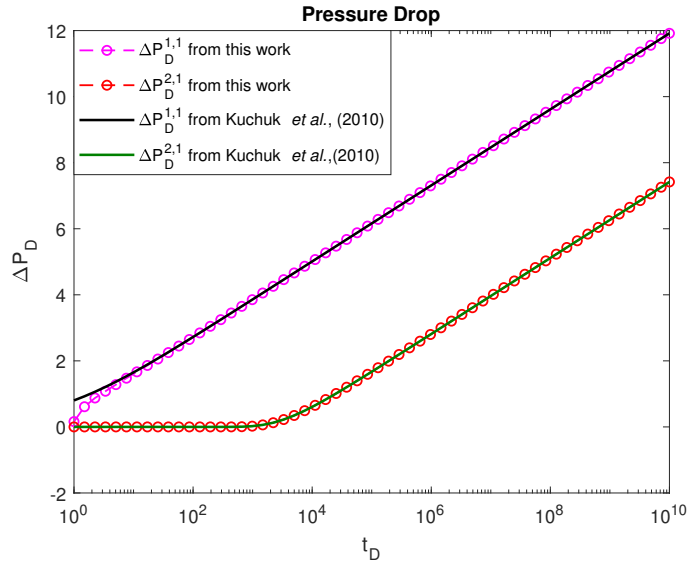
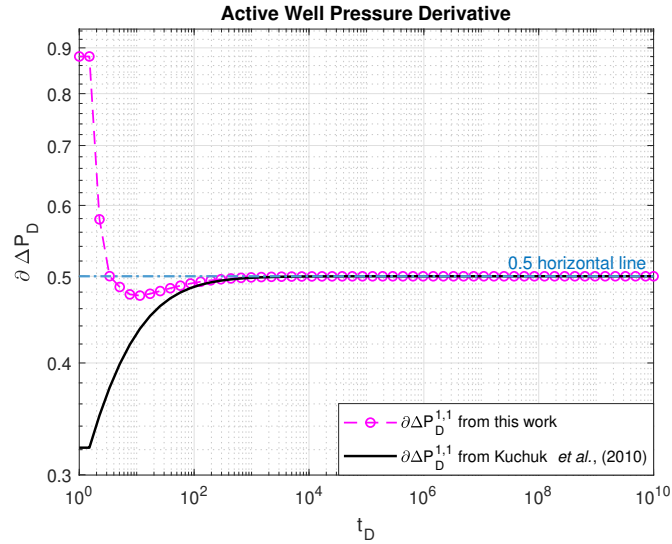
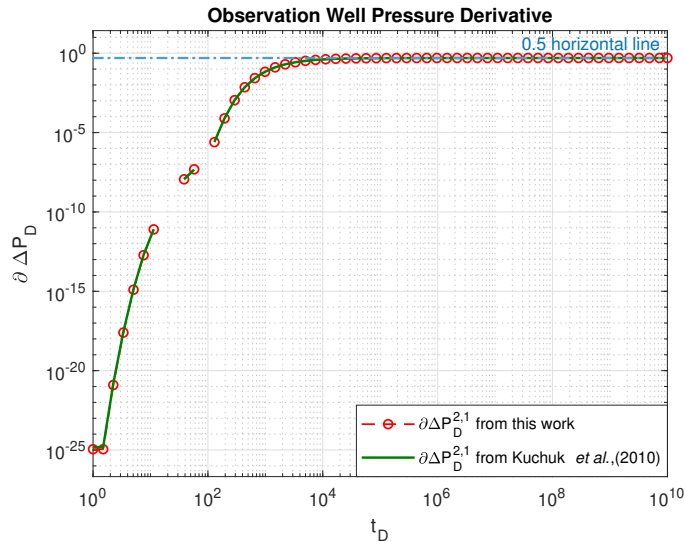


Figure 5.1: Semi-log plot comparing dimensionless pressure values in an infinite homogeneous reservoir for the Example 5.1.1. The graph presents the results from [19] and this work, calculated by Equations (3-32) and (3-34), in a two-well system.

In Figure 5.2, the derivative curves converge nicely to a 0.5 horizontal line. It means that the logarithmic pressure derivative from this work reaches an infinite-acting radial flow regime for both wells, in conformity with [19]. The pressure derivative behavior for the active well ($\partial\Delta P_D^{1,1}$), Figure 5.2(a), identified by pink circles, just like the pressure transient response event, shows a divergence in the early periods owing to the position of the source in time and the exponential function. The observation well outcomes, designated by red circles and dark green solid line in Figure 5.2(b), demonstrate an optimal alignment between the solutions, with minimal discrepancies at the initial times.



5.2(a): Active well Pressure Derivative Plots



5.2(b): Observation well Pressure Derivative Plots

Figure 5.2: Log-log plot of dimensionless pressure derivative vs. time for active and observation well in an infinite homogeneous reservoir for the Example 5.1.1.

The pressure resultant at the spatial position $r_D = D$ is obtained by computing p-p convolution between the \mathcal{G} -function of the system (Equation (3-41)) and the pressure at the dimensionless wellbore radius location, $r_D = 1.0$. The \mathcal{G} -function behavior can provide the flow-regime identification and the diagnosis of the interpretation model to be employed in parameter estimation [19]. The Bourdet derivative, the $t\mathcal{G}$ -function, is also applied for model interpretation purposes via analyses of its log-log curve. The pair of Figures 5.3(a) and 5.3(b) display in sequence the \mathcal{G} -function and $t\mathcal{G}$ -function conduct for the two-well interference test studied.

This study's \mathcal{G} -function curve, marked by pink circles in Figure 5.3(a), closely fits the [19] output (represented by a solid black line) with a negative unit slope marking the onset of the radial flow regime, as expected. It is noticeable that during the late stages, the slope of the curve cuts through the grid cell, dividing its 90-degree angles approximately in half. As a result, calculating the arc-tangent of -45° can confirm the presence of the negative unit slope.

Figure 5.3(b)'s $t\mathcal{G}$ -function plot shows a similar trend, with a great match between the results of this work and from [19] and the possibility of identifying the flow regime from the curve's slope, which suggests the flow phase radial, as the behavior of the graph of $t\mathcal{G}$ -function asymptotically approaches the zero-slope line at the end-stage.

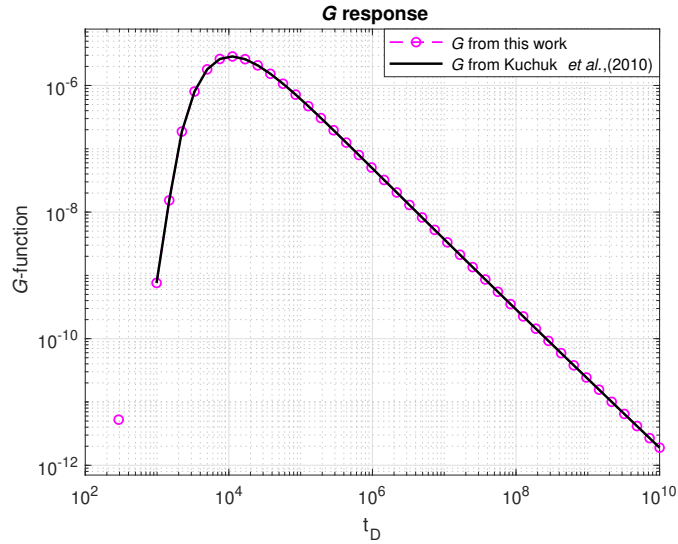
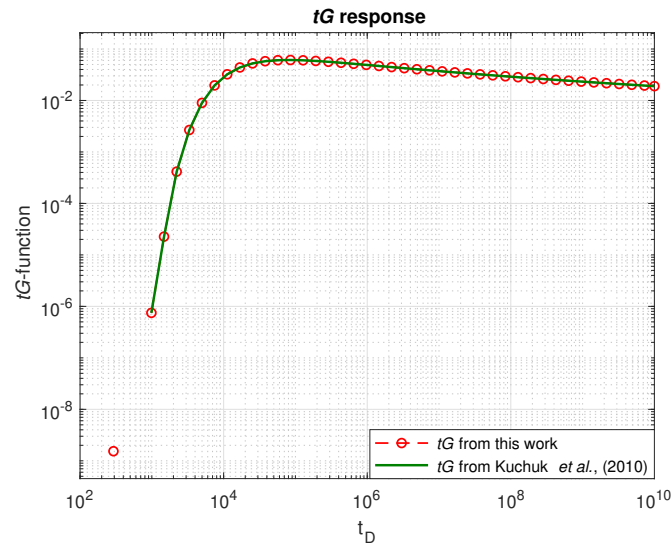
5.3(a): Log-log plot of \mathcal{G} -function5.3(b): Log-log plot of $t\mathcal{G}$ -function

Figure 5.3: Log-log plot of the \mathcal{G} -function and the logarithmic derivative $t\mathcal{G}$ -function vs. time for two-well testing in an infinite homogeneous reservoir for the Example 5.1.1.

5.1.2 Example 2

In the second example, there is an increased distance between the wells, and the radius separating the two media is also wider. The active well was chosen from the observation well at a dimensionless distance $D = 230.0$. The interface, which separates the two different regions, has a radius size of $r_{1D} = 80.0$. The other reservoir properties are the same as in Example 5.1.1.

Figure 5.4 shows the graphical representation of dimensionless pressure data. The dashed line with a circle marker denotes the results obtained by this research work. In contrast, the solid line represents the outcomes derived from the reference [19]. Once again, a satisfactory agreement between the responses can be observed, except for the initial times at the production well ($\Delta P_D^{1,1}$). The impulse action influences these early-time responses in the source at $r'_D = 1.0$ and $t'_D = 1.0$, as demonstrated in the Example 5.1.1.

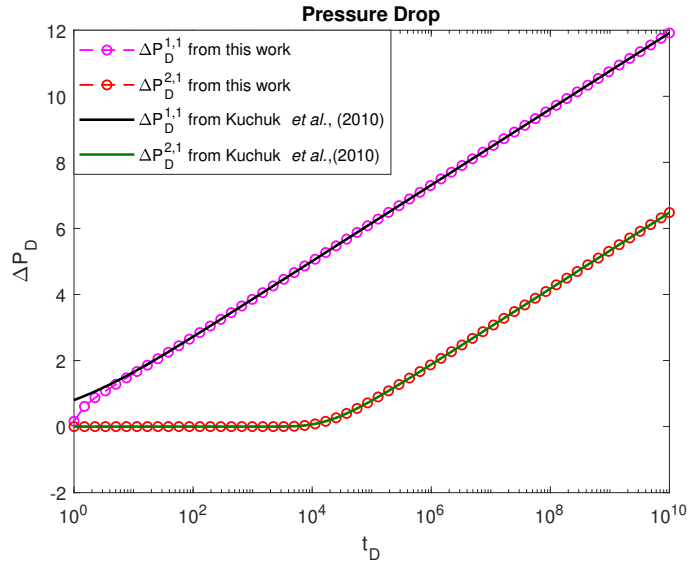
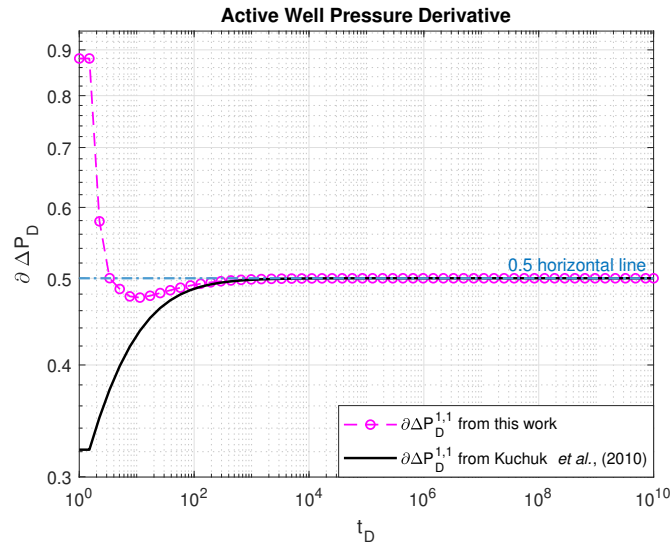
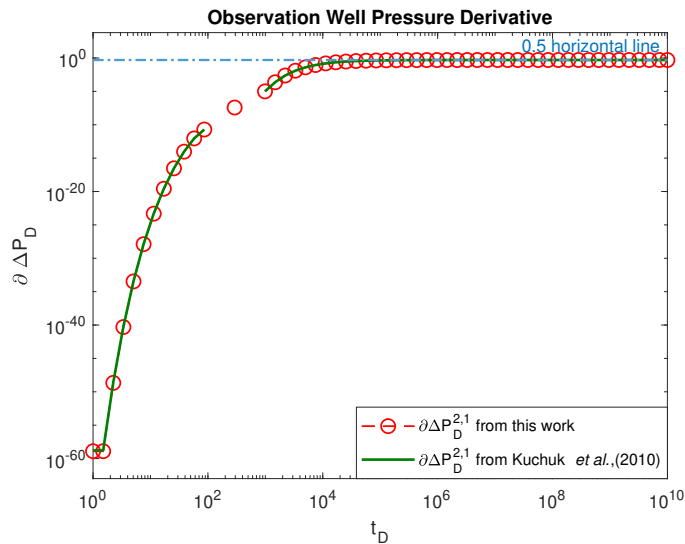


Figure 5.4: Semi-log plot comparing dimensionless pressure values in an infinite homogeneous reservoir for the Example 5.1.2. The graph presents the results from [19] and this work.

Regarding the pressure derivative, Figure 5.5 illustrates the log-log plots of dimensionless pressure derivative data and dimensionless time. For both the producer well and the observation well (Figures 5.5(a) and 5.5(b), in order), the results suggest an infinite-acting radial flow where the curves tend towards a straight horizontal line with a y-intercept of 0.5, which is the expected outcome [19]. And similar to Example 5.1.1, the initial times deviate from that constant level as a consequence of the source situation for the active well while having a negligible influence on the observation well.



5.5(a): Active well Pressure Derivative Plots



5.5(b): Observation well Pressure Derivative Plots

Figure 5.5: Log-log plot of dimensionless pressure derivative vs. time for active and observation well in an infinite homogeneous reservoir for the Example 5.1.2.

The shape of the log-log chart of the functions \mathcal{G} and $t\mathcal{G}$ are depicted in Figures 5.6(a) and 5.6(b) demonstrate conformity with the features presented by the functions \mathcal{G} and $t\mathcal{G}$ in Section 5.1.1. Both functions indicate the presence of a radial flow regime during later stages. This is evidenced by the \mathcal{G} -function's line with an inclination of approximately -45° and the $t\mathcal{G}$ function's line with an inclination of roughly 0° as indicated by Kuchuk et al. [19].

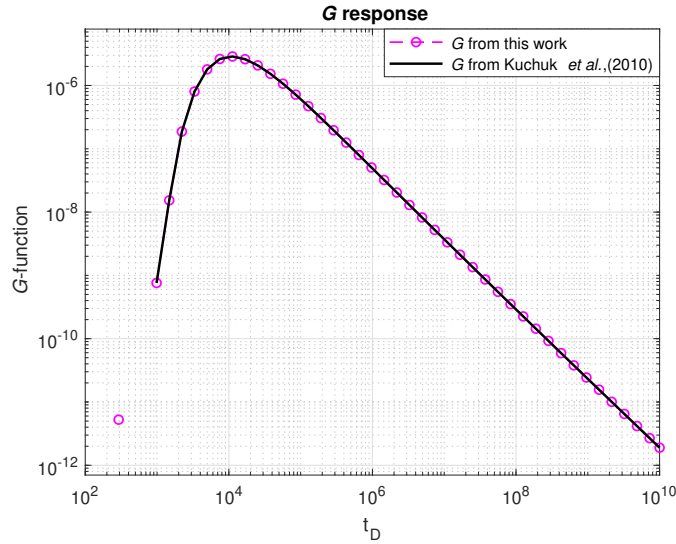
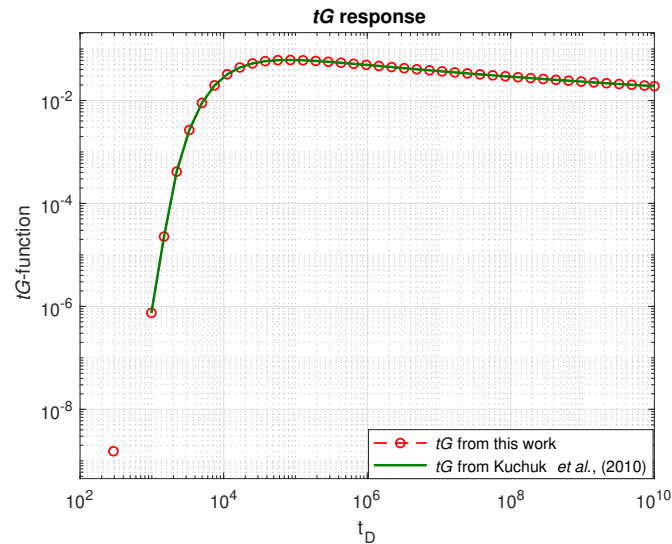
5.6(a): Log-log plot of \mathcal{G} -function5.6(b): Log-log plot of $t\mathcal{G}$ -function

Figure 5.6: Log-log plot of the \mathcal{G} -function and the logarithmic derivative $t\mathcal{G}$ -function vs. time for two-well testing in an infinite homogeneous reservoir for the Example 5.1.2.

5.2

Comparing the Results of the Heterogeneous Scenario

In a scenario characterized by heterogeneity, the rock parameters exhibit variations across different reservoir sections. Thus, two examples illustrate the heterogeneous outcomes by incorporating different permeability values. These examples illustrate the impact of variability on pressure behavior. In both examples, the monitoring well is positioned at a dimensionless distance of $D = 291.06$ from the operating well, with an interface radius with measures

$r_{1D} = 68.15$. The source is positioned at $r'_D = 1.0$ and $t'_D = 0.0$. The parameters are listed in Table 5.2. This analysis will also disregard storage and skin effects like the approach used in the previous section (Section 5.1).

Case	Region	$\kappa [mD]$	$\mu [cP]$	$h [m]$	ϕ	$c_t [cm^2/kgf]$
5.2.1	I	500	5.1	25.0	0.3	2.342×10^{-4}
	II	2000				
5.2.2	I	2000	5.1	25.0	0.3	2.342×10^{-4}
	II	500				

Table 5.2: Reservoir properties for heterogeneous medium.

5.2.1

Example 1

Figure 5.7 displays the dimensionless pressure response of a two-zone composite reservoir. The charts compare the solutions from the reservoir simulator and the outcomes of the suggested model, computed using Equations (3-39) and (3-40) assuming regions with different permeabilities in a two-well system. The solid black line and pink circles graphs point out the measured pressure at the operation well ($\Delta P_D^{1,1}$). The solid dark green line and red circles graphs reference the pressure response at the monitoring well ($\Delta P_D^{2,1}$). The inflection points observed at the $\Delta P_D^{1,1}$ curves mean a shift in permeability across the medium. The graphs show a remarkable similarity between the data collected from both sources.

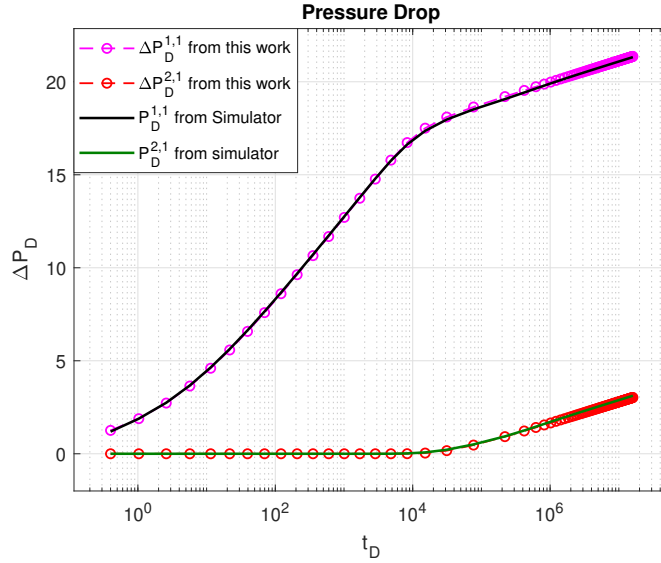
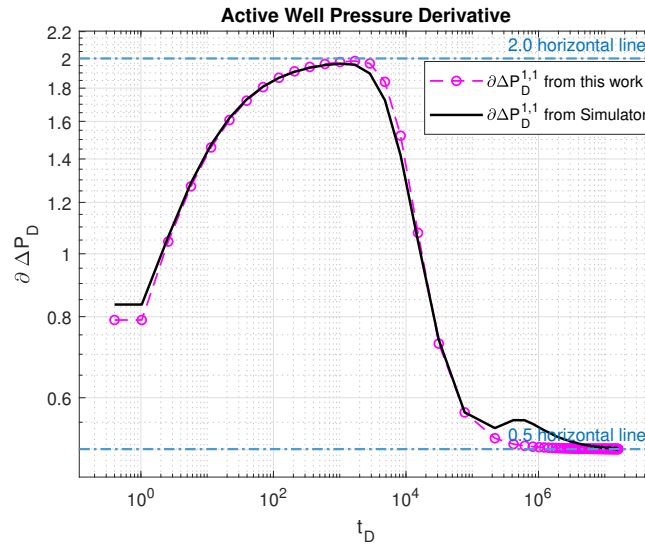
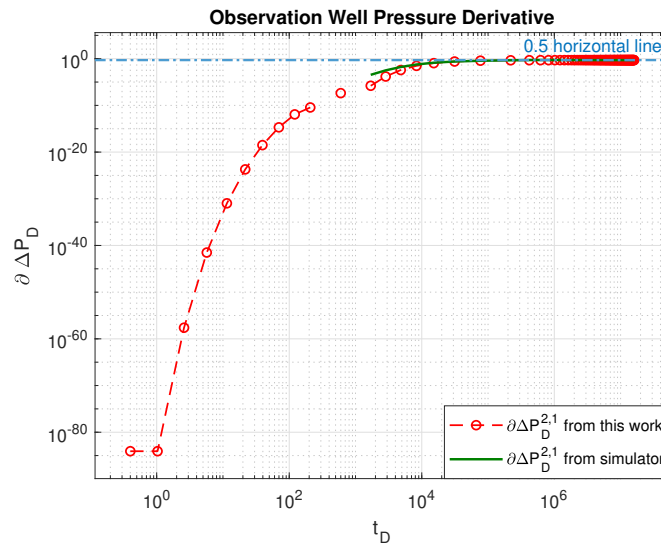


Figure 5.7: Semi-logarithmic plot comparing the dimensionless pressure values for a two-well interference testing in an infinite heterogeneous reservoir for the Example 5.2.1. The plot shows the results from the reservoir simulator solution alongside the outcomes generated by the proposed model for an infinite heterogeneous reservoir.

The log-log plot of the dimensionless pressure derivative for both wells can be verified in Figures 5.8(a) and 5.8(b). The chart displays an upswing of the derivative response values up to the horizontal line at $y = 2.0$, characterizing a relationship where one permeability is four times greater than the other, as shown in Table 5.2. Afterward, the values decrease and converge to the horizontal line $y = 0.5$, indicating an infinite-acting radial flow [19]. When comparing the values of the derivatives, slight dissimilarity can be observed, primarily caused by differences in the treatment of the numerical tests, like the approximation error. In the derivative pressure values at the observation well ($\partial\Delta P_D^{2,1}$), it is apparent that the simulator's curve is absent during the initial times. The simulator does not provide derivative values at the early stages because it outputs zero values. However, this differs from the proposed model's numerical experiments, where the values are very close to zero. In addition, similarly to the derivative pressure value in the active well, the values in the observation well also stabilize around the threshold of 0.5.



5.8(a): Active well Pressure Derivative Plots



5.8(b): Observation well Pressure Derivative Plots

Figure 5.8: Log-log plot of dimensionless pressure derivative vs. time for active and observation well in interference testing in an infinite heterogeneous reservoir for the Example 5.2.1.

Figures 5.9(a) and 5.9(b) exhibit the \mathcal{G} and $t\mathcal{G}$ graph produced by the model proposed in this work. As time progresses, the \mathcal{G} -function gradually approaches a line with a negative unit-slope, while the $t\mathcal{G}$ -function conforms to a line with a zero-slope. These observations align with the expected pattern for an infinite radial flow regime [19].

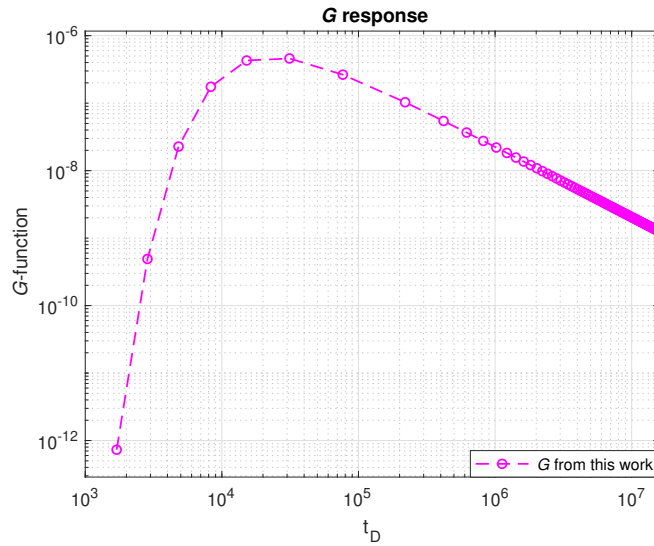
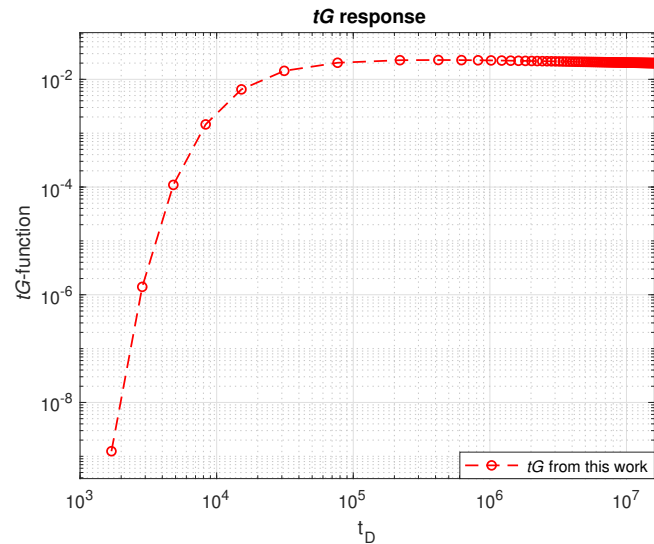
5.9(a): Log-log plot of \mathcal{G} -function5.9(b): Log-log plot of $t\mathcal{G}$ -function

Figure 5.9: Log-log plot of the \mathcal{G} -function and the logarithmic derivative $t\mathcal{G}$ -function vs. time for a two-well interference testing in an infinite heterogeneous reservoir for the Example 5.2.1.

5.2.2 Example 2

As in Example 5.2.1, the measurement for D is 291.06, while r_{1D} measures 68.15. Based on the information in Table 5.2, the inner region has a higher permeability.

Figure 5.10 displays the trends of dimensionless pressure values over time for both the active and observation well. The solid lines indicate the pressure data collected from the simulator, and the circular graphs are based on the

numerical results obtained in this study. The resultant pressure data from both origins exhibit similar behavior and are closely aligned.

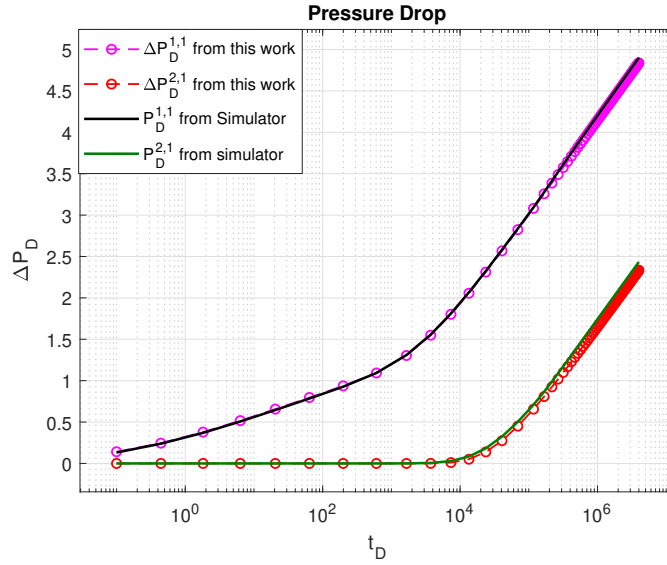
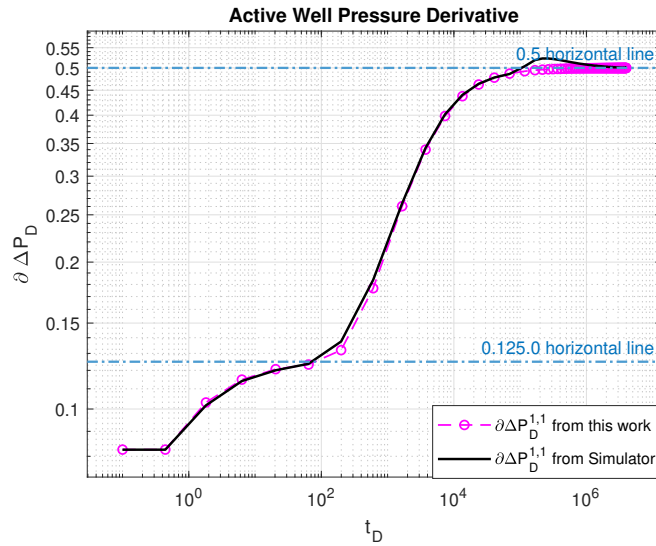
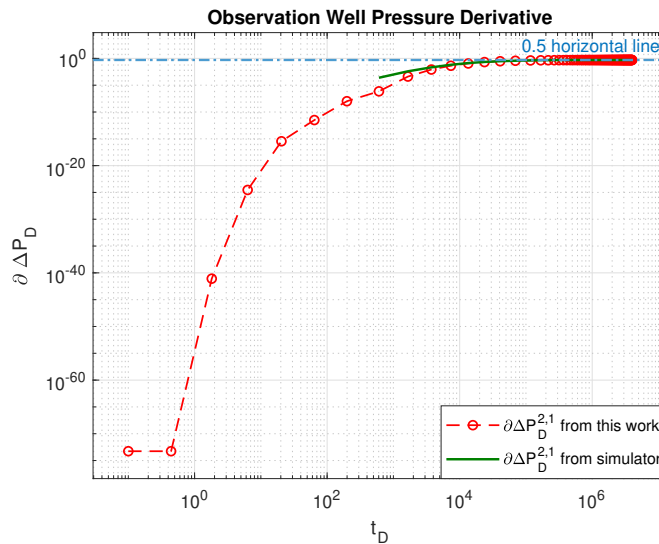


Figure 5.10: Semi-logarithmic plot comparing the dimensionless pressure values for a two-well interference testing in an infinite heterogeneous reservoir for the Example 5.2.2. The plot includes results from the reservoir simulator and the outcomes for an infinite heterogeneous reservoir obtained from the proposed model.

Figures 5.11(a) and 5.11(b) depict the log-log derivative plot arrangement. Both solutions exhibit a horizontal asymptote given by the function $y = 0.5$, denoting an infinite-acting radial flow regime [19]. Initially, for $\partial\Delta P_D^{1,1}$ (Figure 5.11(a)), the pressure differential increases until it reaches the threshold of 0.125, indicated by the dotted horizontal line. It reveals a 1 : 4 inverse proportionality between the internal and external regions. Afterward, the pressure continues to increase and levels off at 0.5. In the case of $\partial\Delta P_D^{2,1}$, like in Example 5.2.1, the pressure derivative values at the observation well, referring to the simulator data, are zero during the initial times. As a result, these values are not present on the graph. Furthermore, the values of the proposed model gradually move towards the 0.5 horizontal line.



5.11(a): Active well Pressure Derivative Plots



5.11(b): Observation well Pressure Derivative Plots

Figure 5.11: Log-log plot of dimensionless pressure derivative vs. time for active and observation well in a two-well interference testing in an infinite heterogeneous reservoir for the Example 5.2.2.

Figures 5.12(a) and 5.12(b) show the \mathcal{G} and $t\mathcal{G}$ graph generated by the proposed model. As time elapses, the \mathcal{G} -function tends towards a negative unit-slope line, while $t\mathcal{G}$ -function asymptotically approaches a zero-slope line, a known pattern for an infinite radial flow regime, as shown by [19].

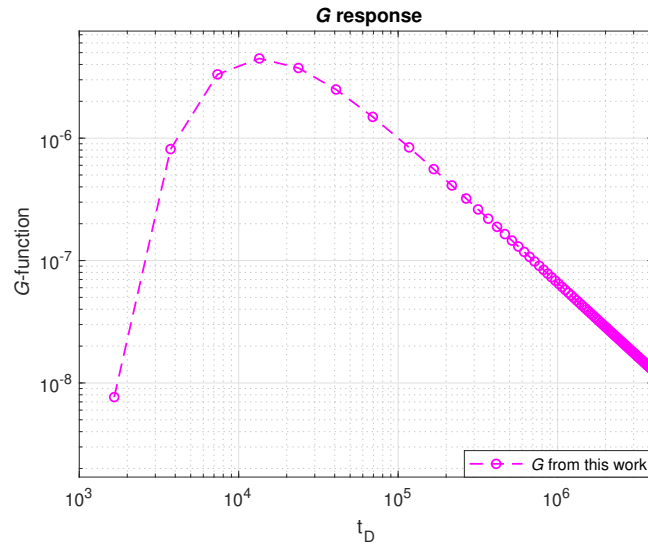
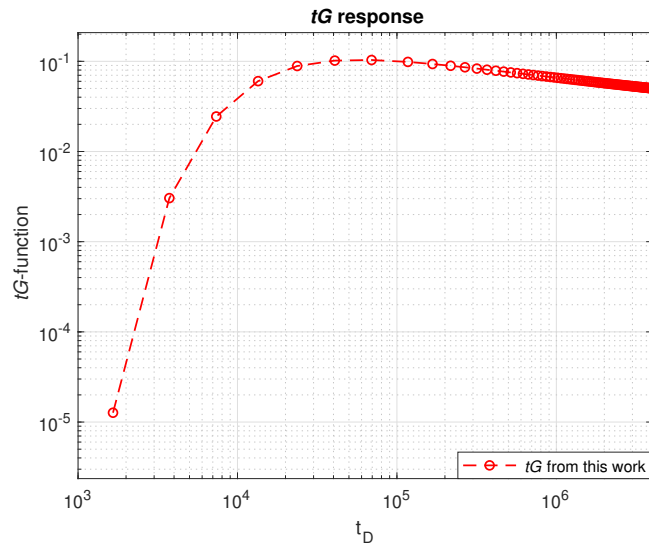
5.12(a): Log-log plot of \mathcal{G} -function5.12(b): Log-log plot of $t\mathcal{G}$ -function

Figure 5.12: Log-log plot of the \mathcal{G} -function and the logarithmic derivative $t\mathcal{G}$ -function vs. time for a two-well interference testing in an infinite heterogeneous reservoir for the Example 5.2.2.

5.3

Comparing the Results of the Two-Phase Scenario

This scenario involves a reservoir that is considered to be homogeneous, with water used as the injected fluid. As a result of the water displacing oil, two zones are formed due to their different properties. The interface radius (r_f) is determined by the advancing front of the water, which is given by Equation (4-1). Consequently, the interface is no longer stationary and becomes a time-dependent function. In addition, a piston-like model is used to estimate

the propagation of the waterfront. $K_{rw} = 1$ if the medium is saturated with water. $K_{ro} = 1$ when water is absent. The monitoring well is positioned at a dimensionless distance of $D = 291.06$ from the operating. The source is positioned at $r'_D = 1.0$ and $t'_D = 0.0$. Table 5.3 lists the parameters applied in the study. This analysis will not assume storage and skin effects like the approach taken in Section 5.2.

Case	Region	κ [mD]	μ [cP]	h [m]	ϕ	c_t [cm^2/kgf]
5.3	I	2000	0.51	25.0	0.3	2.342×10^{-4}
	II		5.1			

Table 5.3: Reservoir properties for a homogeneous medium under two-phase flow.

Figure 5.13 depicts the behavior of dimensionless pressure values over time for injecting and monitoring wells. The continuous lines represent the pressure data acquired from the simulator, while the circular graphs correspond to the numerical outcomes derived from this investigation. The graphs show a consistent pattern with a slight disparity in pressure values in later stages.

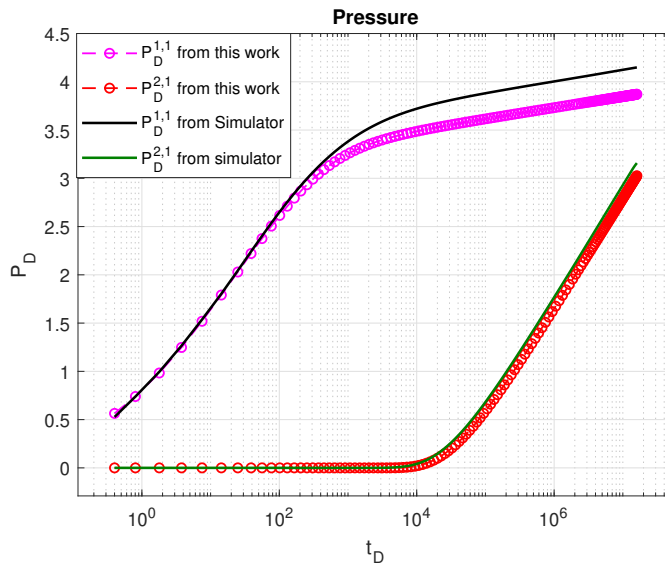
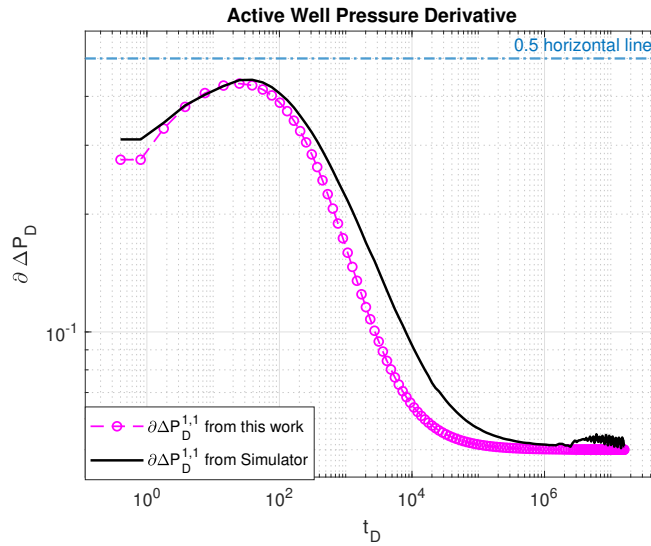


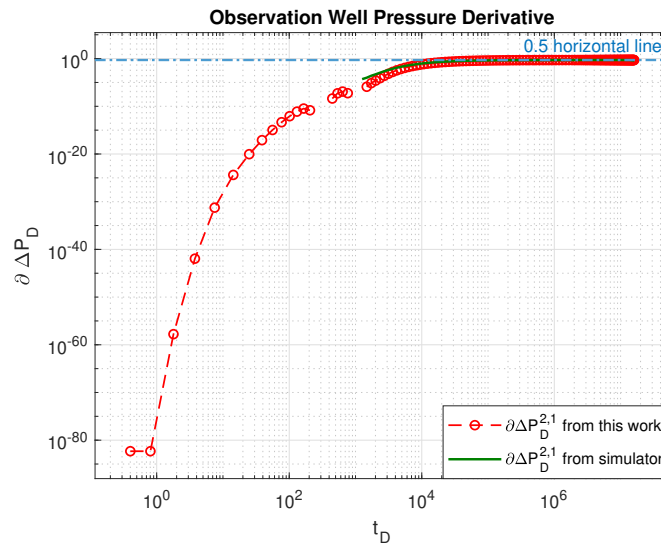
Figure 5.13: Semi-logarithmic plot comparing the dimensionless pressure values for a two-well interference testing in an infinite homogeneous reservoir during two-phase flow for the Example 5.3. The plot includes results from the reservoir simulator and those from an infinite two-phase system obtained from the proposed model.

Figures 5.14(a) and 5.14(b) depict the log-log derivative graph. The function $y = 0.5$ is initially approached by the derivative $\partial\Delta P_D^{1,1}$ (Figure

5.14(a)) due to dimensionless modeling by oil properties and fluid distribution over time. The variation in values within the transition region may be due to the different calculation methodologies used by the simulator compared to the approach adopted in this study. Furthermore, the reservoir simulators calculate the average pressure in different blocks. Discretizations may not fully capture variations, leading to significant errors in pressure estimation in regions with abrupt changes in reservoir properties. For $\partial\Delta P_D^{2,1}$ (observe 5.14(b)), as seen in Example 5.2, the pressure derivative values from the simulator are initially zero at the observation well. Therefore, these values are not displayed on the graph. The proposed model's values also converge to $y = 0.5$, indicating an infinite-acting radial flow regime [19].



5.14(a): Active well Pressure Derivative Plots



5.14(b): Observation well Pressure Derivative Plots

Figure 5.14: Log-log plot of dimensionless pressure derivative vs. time for a two-well interference testing in an infinite homogeneous reservoir during two-phase flow for the Example 5.3.

Figures 5.15(a) and 5.15(b) show the graphs for \mathcal{G} and $t\mathcal{G}$ resulting from the proposed model. The \mathcal{G} -function values converge to a unit line of negative slope over time, while the $t\mathcal{G}$ -function approaches a zero-slope line in the end stages with a slight deviation. This deviation is minor enough to preserve the characteristic behavior of an infinite radial regime [19].

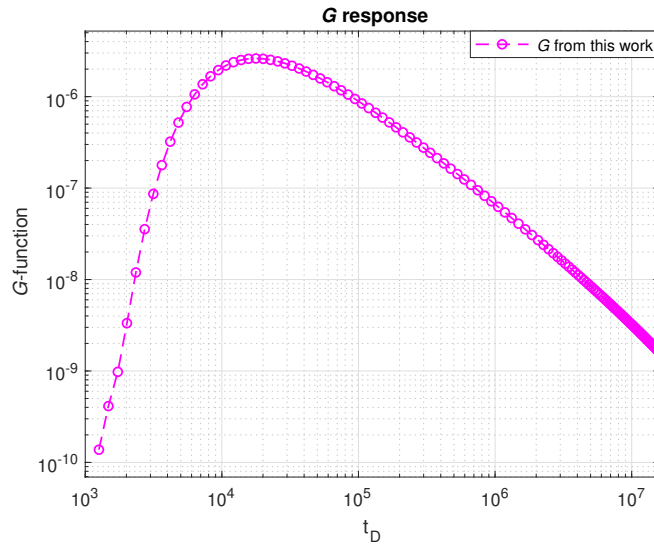
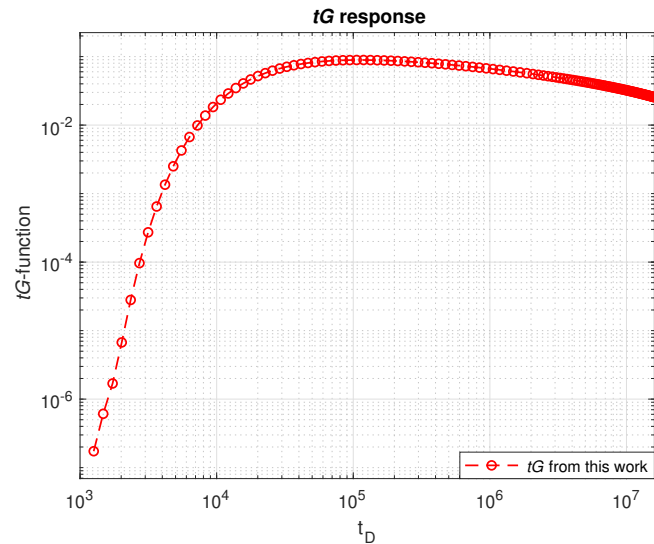
5.15(a): Log-log plot of \mathcal{G} -function5.15(b): Log-log plot of $t\mathcal{G}$ -function

Figure 5.15: Log-log plot of the \mathcal{G} -function and the logarithmic derivative $t\mathcal{G}$ -function vs. time for a two-well interference testing in an infinite homogeneous reservoir during two-phase flow for the Example 5.3.

The results show close alignment upon comparison, indicating that the proposed model is reliable and consistent and can be a valuable tool for analyzing and predicting pressure behavior without accurate flow rate data.

6

Conclusion and future work

This study proposes a novel technique for interpreting well testing in a composite reservoir system. The suggested approach involves simultaneously utilizing a radially composite reservoir model with the pressure-pressure convolution method [17] to obtain pressure behavior for heterogeneous reservoirs and homogeneous reservoirs during a two-phase flow while circumventing any uncertainties that may arise from flow rate measurements. The composite reservoir comprises two distinct regions, each with its own well: an operation well in the inner region and a monitoring well in the outer region (see Figures 3.3 and 4.2). In this process, a unit rate production source is positioned in the active well to engender a response in the system. Next, the unit impulse response, also called Green's function, is calculated to depict how each well in the system responds to this influence. This information is used to establish the *kernel* of the pressure-pressure (p-p) convolution, which enables the diagnosis of reservoir parameters and the flow regime and the determination of pressure changes at both wellbores.

Three steps were used to validate the proposed solution. The first method involved directly comparing the results of the homogeneous model - the line-source solution - with those previously published by Kuchuk et al. [19]. The second method involved comparing the outputs of a commercial simulator based on finite differences with this study's outcomes for a heterogeneous and a two-phase model by analyzing their respective behaviors.

In the homogeneous case, two examples were provided. The first example had a smaller interface radius and well spacing than the second one. The findings of both examples were great when compared to the numerical results derived from Kuchuk et al. [19]. Although the findings at the initial times reveal a slight disparity due to the source's activity, a great agreement was observed between the numerical data.

The analysis of the system's heterogeneity was also conducted based on two examples. The heterogeneity was incorporated by assigning different permeability values to each zone of the composite reservoir. In the first example, the internal region was assigned a permeability value four times smaller than the external region's. In contrast, in the second example, the

internal zone's permeability value was four times higher than in the outer zone. This relationship between the permeability information, directly or inversely in a four-to-one ratio, is reflected in the pressure derivative data. Furthermore, \mathcal{G} -function and $t\mathcal{G}$ -function exhibited a quite fitting behavior in line with what is presented in the literature.

The findings from the two-phase scenario, which incorporates variations in fluid properties and the dynamic movement of the waterfront radius during injection, align consistently with the calculated outputs from the flow simulator. \mathcal{G} -function and its Bourdet derivative also revealed appropriate behavior in line with established literature.

After comparing the results, it is noticeable that they are closely matched, suggesting that the proposed model holds great promise and can be an effective tool for analyzing and predicting pressure behavior even without flow rate information.

For future work, we intend to expand the developed model, including the effects of skin and wellbore storage, which were neglected in this study. Addressing these effects is significant because during an interference test, the impulse response function, \mathcal{G} -function, can be affected by the wellbore storage at the monitoring well and the skin factor at the operation well. The proposed model can incorporate both of these conditions. One can use the expression developed by Van Everdingen & Hurst (1949) [28] to account for wellbore storage. To account for the impact of skin effect on the model, a three-zone radially composite model can be adopted [15]. This model includes the skin parameters within the inner zone. By implementing these changes, the model for analyzing transient pressure when flow data is unavailable or uncertain will become more robust.

In addition, the model presented provides a flexible solution for applications that depend on radially composite-based approaches, such as modeling two-phase flow in multilayer reservoirs. It can be achieved because the pressure data can be collected horizontally or vertically within a formation for pressure-pressure convolution, as mentioned in this study.

Bibliography

- [1] SATTER, A.; IQBAL, G. M.. **Waterflooding and waterflood surveillance**. In: RESERVOIR ENGINEERING, p. 289–312. Gulf Professional Publishing, Boston, 2016.
- [2] ABBASZADEH, M.; KAMAL, M.. **Pressure-transient testing of water-injection wells**. SPE Reservoir Engineering, 4:115–124, 02 1989.
- [3] BARRETO, A. B.; PERES, A. M. M. ; PIRES, A.. **Water injectivity tests on multilayered oil reservoirs**. In: BRASIL OFFSHORE. OnePetro, 2011.
- [4] PERES, A. M. M.; REYNOLDS, A. C.. **Theory and Analysis of Injectivity Tests on Horizontal Wells**. SPE Journal, 8(02):147–149, 06 2003.
- [5] PERES, A. M. M.; BOUGHRARA, A. A.; CHEN, S.; MACHADO, A. A. V. ; REYNOLDS, A. C.. **Approximate Analytical Solutions for the Pressure Response at a Water Injection Well**. volumen All Days de SPE Annual Technical Conference and Exhibition, p. SPE–90079–MS, 09 2004.
- [6] OLAREWAJU, J. S.; LEE, J. W.. **A Comprehensive Application of a Composite Reservoir Model to Pressure-Transient Analysis**. SPE Reservoir Engineering, 4(03):325–331, 1987.
- [7] KUCHUK, F. J.; HABASHY, T. M.. **Solution of pressure diffusion in radially composite reservoirs**. Transport in porous media, 19:199–232, 1995.
- [8] VIANA, I.; V., R.; PESCO, S. ; BARRETO, A. B.. **An analytical model for pressure behavior in multilayered radially composite reservoir with formation crossflow**. Journal of Petroleum Exploration and Production Technology, p. 1–13, 2022.
- [9] CAO, C.; CHENG, L.; JIA, P.; SHI, J. ; DEGHANPOUR, H.. **A dynamic fracture model combining with laplace transform and synchronous iteration method for transient behavior analysis of a four-zone system**. Journal of Hydrology, 615:128723, 2022.

- [10] LOUCKS, T. L.; GUERRERO, E. T.. **Pressure Drop in a Composite Reservoir**. Society of Petroleum Engineers Journal, 1(03):170–176, 09 1961.
- [11] SATMAN, A.. **An Analytical Study of Interference in Composite Reservoirs**. Society of Petroleum Engineers Journal, 25(02):281–290, 04 1985.
- [12] THOMPSON, L. G.; REYNOLDS, A. C.. **Well Testing for Radially Heterogeneous Reservoirs Under Single and Multiphase Flow Conditions**. SPE Formation Evaluation, 12(01):57–64, 03 1997.
- [13] YAN, Z.; CAO, C.; XIE, M.; JIA, P.; LIU, G.; WEI, X.; CHENG, L. ; TU, Z.. **Pressure behavior analysis of permeability changes due to sand production in offshore loose sandstone reservoirs using boundary-element method**. Geofluids, 2021:1–10, 2021.
- [14] MASTBAUM, A.; SOUZA, A.; NETO, J. L. F. B.; BELA, R. V. ; BARRETO, A. B.. **Dual-phase flow in two-layer porous media: a radial composite laplace domain approximation**. Journal of Petroleum Exploration and Production Technology, 11, 2021.
- [15] BITTENCOURT NETO, J. L. F.; BELA, R. V.; PESCO, S. ; BARRETO, A. B.. **Pressure Behavior During Injectivity Tests - A Composite Reservoir Approach**. SPE Latin America and Caribbean Petroleum Engineering Conference, 2020.
- [16] BELA, R. V.; PESCO, S. ; BARRETO, A. B.. **Impulse functions applied to compute pressure change during injectivity tests**. Fuel, 310:122392, 2022.
- [17] GOODE, P. A.; POP, J. J. ; MURPHY, W. F., I.. **Multiple-Probe Formation Testing and Vertical Reservoir Continuity**. volumen All Days de SPE Annual Technical Conference and Exhibition, 10 1991.
- [18] ONUR, M.; HEGEMAN, P. S. ; KUCHUK, F. J.. **Pressure/Pressure Convolution Analysis of Multiprobe and Packer-Probe Wire-line Formation Tester Data**. SPE Reservoir Evaluation Engineering, 7(05):351–364, 10 2004.
- [19] KUCHUK, F. J.; ONUR, M. ; HOLLAENDER, F.. **Pressure transient formation and well testing: convolution, deconvolution and non-linear estimation**. Elsevier, 2010.

- [20] STEHFEST, H.. **Algorithm 368: Numerical inversion of laplace transforms [d5]**. Communications of the ACM, 13(1):47–49, 1970.
- [21] BOURDET, D.; AYOUB, J. A. ; PIRARD, Y. M.. **Use of Pressure Derivative in Well-Test Interpretation**. SPE Formation Evaluation, 4(02):293–302, 1989.
- [22] SMITH, S. W.. **Digital signal processing: a practical guide for engineers and scientists**. Elsevier Science, 2003.
- [23] LATHI, B. P.; GREEN, R. A.. **Signal processing and linear systems, volumen 2**. Oxford University Press Oxford, 1998.
- [24] KUCHUK, F. J.. **Applications of Convolution and Deconvolution to Transient Well Tests**. SPE Formation Evaluation, 5(04):375–384, 12 1990.
- [25] HAHN, D. W.; ÖZISIK, M. N.. **Heat conduction**. John Wiley & Sons, 2012.
- [26] COLE, K.; BECK, J.; HAJI-SHEIKH, A. ; LITKOUHI, B.. **Heat conduction using Greens functions**. Taylor & Francis, 2010.
- [27] DUFFY, D. G.. **Green’s functions with applications**. Chapman and Hall/CRC, 2nd. edition, 03 2015.
- [28] VAN EVERDINGEN, A. F.; HURST, W.. **The Application of the Laplace Transformation to Flow Problems in Reservoirs**. Journal of Petroleum Technology, 1(12):305–324, 12 1949.
- [29] ODEH, A. S.; JONES, L. G.. **Pressure Drawdown Analysis, Variable-Rate Case**. Journal of Petroleum Technology, 17(08):960–964, 08 1965.
- [30] THOMPSON, L. G.; REYNOLDS, A. C.. **Analysis of Variable-Rate Well-Test Pressure Data Using Duhamel’s Principle**. SPE Formation Evaluation, 1(05):453–469, 10 1986.
- [31] ONUR, M.; AYAN, C. ; KUCHUK, F. J.. **Pressure-Pressure Deconvolution Analysis of Multiwell-Interference and Interval-Pressure-Transient Tests**. SPE Reservoir Evaluation Engineering, 14(06):652–662, 12 2011.
- [32] GRINGARTEN, A. C.; RAMEY JR, H. J.. **The use of source and green’s functions in solving unsteady-flow problems in reservoirs**. Society of Petroleum Engineers Journal, 13(05):285–296, 1973.

- [33] ABRAMOWITZ, M.; STEGUN, I. A.. **Handbook of mathematical functions with formulas, graphs, and mathematical tables**, volumen 55. US Government printing office, 1964.
- [34] BUCKLEY, S. E.; LEVERETT, M. C.. **Mechanism of fluid displacement in sands**. Transactions of the AIME, 146(01):107–116, 1942.

A Derivation of the Pressure-Pressure Convolution Equations

This appendix presents a detailed development of the pressure-pressure convolution formulation discussed in Chapter 2.

A two-dimensional infinite radial model is assumed (Fig. 2.3), comprising an active well and an observation well separated by a distance of D . In this model, wellbore storage and skin effects are not considered. Thus, the p-r convolution for the active well in the time domain can be calculated using the following equation:

$$\Delta p_1(r_w, t) = \int_0^t q_1(\tau) g_{1,1}(r_w, t - \tau) d\tau \quad (\text{A-1})$$

After applying the Laplace transform,

$$\Delta \bar{p}_1(r_w, u) = \bar{q}_1(u) \bar{g}_{1,1}(r_w, u), \quad (\text{A-2})$$

Similarly, at the observation well, the pressure response in the time domain can be obtained by:

$$\Delta p_2(D, t) = \int_0^t q_1(D, \tau) g_{2,1}(t - \tau) d\tau \quad (\text{A-3})$$

Upon performing the Laplace transform, the result is as follows:

$$\Delta \bar{p}_2(D, u) = \bar{q}_1(u) \bar{g}_{2,1}(D, u) \quad (\text{A-4})$$

In the given context, the subscripts 1 and 2 are associated with W_1 and W_2 , respectively. q_1 represents the production rate at the active well. Furthermore, $g_{1,1}$ denotes the unit-impulse response at the active well caused by the constant source. Additionally, $g_{2,1}$ refers to the unit-impulse response at the observation well, W_2 , resulting from production at W_1 . Additionally, u

represents the Laplace variable, and the overlined variables indicate that they are in the Laplace domain.

Equations (A-2) and (A-4) share the flow-rate term. So, dividing one equation by the other leads to the subsequent formulation:

$$\Delta \bar{p}_2(D, u) = \Delta \bar{p}_1(r_w, u) \frac{\bar{g}_{2,1}(D, u)}{\bar{g}_{1,1}(r_w, u)} \quad (\text{A-5})$$

B The Auxiliary Problem for Green's Function

This appendix explains how Green's function definition is associated with the dimensionless government equations presented in Equations (3-6) and (3-7), along with their initial, boundary, and interface conditions, respectively defined in Equations (3-8) - (3-12). The goal is to determine Green's function G , which satisfies Equation (3-13) and produces the pressure-pressure convolution kernel.

The source is located only in the area between r_w and r_1 as illustrated in Figure 3.2. Outside of this zone, there is no source. The impulse response in Region I, denoted by $G_{1,1}$, and in Region II, indicated as $G_{2,1}$, results from this source. As a consequence, the dimensionless equations that govern Region I and II are stated as:

– Region I ($1 < r'_D, r_D < r_{1D}$):

$$\begin{aligned} \frac{1}{r_D} \frac{\partial}{\partial r_D} \left(r_D \frac{\partial G_{1,1}(r_D, r'_D, t_D, t'_D)}{\partial r_D} \right) - \frac{\eta_2}{\eta_1} \frac{\partial G_{1,1}(r_D, r'_D, t_D, t'_D)}{\partial t_D} = \\ = -\frac{\kappa_2}{\kappa_1} \delta(r_D - r'_D) \delta(t_D - t'_D); \quad (\text{B-1}) \end{aligned}$$

– Region II ($r'_D < r_{1D} < r_D < r_{eD}$):

$$\frac{1}{r_D} \frac{\partial}{\partial r_D} \left(r_D \frac{\partial G_{2,1}(r_D, r'_D, t_D, t'_D)}{\partial r_D} \right) - \frac{\partial G_{2,1}(r_D, r'_D, t_D, t'_D)}{\partial t_D} = 0; \quad (\text{B-2})$$

It is possible to see in Equation (B-1) the presence of the source on the right side of the equation, whereas in Equation (B-2), the absence of the source is noticeable.

The initial conditions are expressed as follows:

$$\text{IC: } G_{1,1}(r_D, r'_D, t_D, t'_D) = G_{2,1}(r_D, r'_D, t_D, t'_D) = 0 \quad t_D < t'_D \quad (\text{B-3})$$

Furthermore, it is noted that $G = 0$ at the boundary by Equation (3-14). Thus, the boundary conditions can be expressed in the succeeding manner:

$$\text{IBC: } \left(r_D \frac{\partial G_{1,1}(r_D, r'_D, t_D, t'_D)}{\partial r_D} \right) \Bigg|_{r_D=1} = 0, \quad 1 < r'_D, r_D < r_{1D}, \quad (\text{B-4})$$

$$\text{OBC: } \lim_{r_{eD} \rightarrow +\infty} G_{2,1}(r_D = r_{eD}, r'_D, t_D, t'_D) = 0 \quad r'_D < r_{1D} < r_D < r_{eD}; \quad (\text{B-5})$$

Applying the Equation (3-13) to the interface conditions yields the following associated problem:

– Interface ($r_D = r_{1D}$):

$$\text{PCC: } G_{1,1}(r_{1D}^-, r'_D, t_D, t'_D) = G_{2,1}(r_{1D}^+, r'_D, t_D, t'_D), \quad (\text{B-6})$$

RCC:

$$\left(r_D \frac{\partial G_{1,1}(r_D, r'_D, t_D, t'_D)}{\partial r_D} \right) \Bigg|_{r_D=r_{1D}^-} = \frac{\kappa_2}{\kappa_1} \left(r_D \frac{\partial G_{2,1}(r_D, r'_D, t_D, t'_D)}{\partial r_D} \right) \Bigg|_{r_D=r_{1D}^+} \quad (\text{B-7})$$

The equations provided in the chapter can be utilized to determine the impulse function for each well in the system.